Meltwater Penetration Through Temperate Ice Layers in the Percolation Zone of the Greenland Ice Sheet

Shawn J. Marshall[1,1], Samira Samimi[1,1], and Michael MacFerrin[2,2]

[1]University of Calgary
[2]University of Colorado Boulder

November 30, 2022

Abstract

Meltwater retention in the firn layer of the Greenland Ice Sheet is has the potential to buffer sea level rise due to ice sheet melt. The capacity of the firn layer to store meltwater is unclear, however, because refrozen ice layers can act as impermeable barriers to meltwater percolation, promoting runoff rather than retention. We present time-domain reflectometry and thermistor data which demonstrates that meltwater successfully penetrates ice layers up to 12 cm thick in the near-surface firn at Dye2, Greenland. Our observations indicate that ice layers within polar firn can become permeable when summer warming and latent heat release from refreezing meltwater raise temperatures to the melting point. This facilitates meltwater retention, and indicates that the depth of penetration of the summer melting front (the 0°C isotherm) represents the primary control on meltwater infiltration in the percolation zone of the Greenland Ice Sheet.

Meltwater Penetration Through Temperate Ice Layers in the Percolation Zone of the Greenland Ice Sheet

Samira Samimi[1], Shawn J. Marshall[1,2] and Michael MacFerrin[3]

[1] Department of Geography, University of Calgary, Calgary, Alberta, Canada
[2] Environment and Climate Change Canada, Gatineau, Quebec, Canada
[3] Cooperative Institute for Research in Environmental Sciences, University of Colorado, USA

Corresponding author: Samira Samimi (samira.samimi@ucalgary.ca)

Key Points:

- Time-domain reflectometry probes give direct measurements of meltwater infiltration in firn on the Greenland Ice Sheet.
- We document meltwater penetration through ice layers up to 12 cm thick in temperate firn.
- The wetting front and melting front were coincident, indicating thermodynamic controls on meltwater infiltration and retention.

Abstract

Meltwater retention in the firn layer of the Greenland Ice Sheet is has the potential to buffer sea level rise due to ice sheet melt. The capacity of the firn layer to store meltwater is unclear, however, because refrozen ice layers can act as impermeable barriers to meltwater percolation, promoting runoff rather than retention. We present time-domain reflectometry and thermistor data which demonstrates that meltwater successfully penetrates ice layers up to 12 cm thick in the near-surface firn at Dye2, Greenland. Our observations indicate that ice layers within polar firn can become permeable when summer warming and latent heat release from refreezing meltwater raise temperatures to the melting point. This facilitates meltwater retention, and indicates that the depth of penetration of the summer melting front (the 0°C isotherm) represents the primary control on meltwater infiltration in the percolation zone of the Greenland Ice Sheet.

Plain Language Summary

Meltwater that percolates below the surface of the Greenland Ice Sheet is difficult to track; some of it contributes to runoff, mass loss, and sea level rise, but some meltwater refreezes and is retained within the system. Greenland has a large firn area, where multi-year snow that has not yet transitioned to glacial ice has pore space that can retain meltwater. To improve understanding of hydrological and mass balance processes in polar firn, we excavated two firn pits in the Greenland Ice Sheet accumulation area in spring, 2016, and instrumented these pits with thermistors and time-domain reflectometry (TDR) sensors, connected to continuously-recording dataloggers. These sensors allowed us to directly track the coupled thermal and hydrological evolution in the firn through the summer melt season. We recorded nearly identical conditions at each site, with evidence of meltwater infiltration to a depth of between 1.8 m and 2.1 m and a wetting front that was thermally controlled, i.e. coincided with the melting front. This included meltwater penetration through numerous ice layers, including layers up to 12 cm thick. All of this meltwater refroze. Our results indicate that ice layers do not always present an impermeable barrier to meltwater percolation and retention.

1 Introduction

Mass loss from the Greenland Ice Sheet has increased in recent decades due to significant increases in surface melt and runoff (van den Broeke *et al*., 2009; Mouginot *et al*., 2019). One of the challenges in estimating the contribution of the ice sheet to sea level rise is the fact that the surface melting does not always lead to runoff. In the percolation zone, surface meltwater that infiltrates the underlying cold snow or firn can be retained as liquid water (Forster et al., 2014; Koenig et al., 2014) or as refrozen ice (Pfeffer et al., 1991; Pfeffer and Humphrey, 1998; Harper et al., 2012). This reduces summer runoff and ice sheet contributions to sea level rise (Harper et al., 2012; Rennerhalm et al., 2013), and meltwater retention processes may be increasingly important as melting propagates to higher elevations in Greenland in a warming world (Vernon et al., 2013).

Meltwater that percolates and refreezes is difficult to account for in altimetric measurements of surface mass balance, as it is not possible to detect how much meltwater is retained within the system. This is also a source of uncertainty in mass balance models, as processes of meltwater percolation and refreezing occur at fine scales, are spatially heterogeneous, and *in situ* observations are scarce (*e.g.*, Harper et al., 2012; van As et al., 2016; Verjans et al., 2019, Vandecrux et al, 2019). This makes it difficult to calibrate and validate models of these processes, particularly on the scale of polar ice caps and ice sheets.

The extent to which meltwater retention in firn can buffer mass loss and sea-level rise is also unclear. Greenland's firn zone covers more than 80% of the ice sheet, but refrozen near-surface ice layers can act as impermeable barriers, redirecting meltwater percolation into runoff (Machguth et al., 2016; Noel et al., 2017; MacFerrin et al., 2019). In the percolation zone, firn densification associated with warming and refreezing is also leading to a loss of available pore space, imposing further limits on meltwater storage capacity as melting progresses inland (Vandecrux et al., 2019). These processes increase the ratio of meltwater runoff to retention. Hence, models of meltwater infiltration also need to account for ice-layer and firn-densification processes. These represent significant uncertainties in projections of the Greenland ice sheet's response to climate warming.

To examine meltwater infiltration and refreezing processes in the Greenland ice sheet percolation zone, we instrumented two firn pits with arrays of thermistors and time-domain reflectometry (TDR) sensors in order to track the coupled thermal and hydrological evolution of near-surface snow and firn through a summer melt season. The TDR sensors provide continuous measurements of dielectric permittivity, a proxy for liquid water content in the snow and firn. This manuscript presents these *in situ* observations and their implications for meltwater retention in firn. The experiment builds on Humphrey et al. (2012), who used thermistor arrays to track the thermal signature of meltwater infiltration in firn, which is apparent through the latent heat release when meltwater refreezes. Through the addition of TDR probes, we directly trace meltwater flow in the near-surface snow and firn. A similar experimental setup in the Canadian Rocky Mountains successfully demonstrated the ability to track meltwater percolation, refreezing, and snow-water content in a supraglacial snowpack using TDR probes (Samimi and Marshall, 2017). The implementation in Greenland extends the earlier experiments to polar firn, where liquid water content is lower and meltwater refreezing is more significant.

2 Methods

Measurements were established in May, 2016 in the near-surface firn at 66˚28′39″N, 46˚17′5″W, near Dye 2 station on the southwestern flank of the Greenland Ice Sheet. The study sites were at an elevation of 2120 m, representing the upper part of the percolation zone in southern Greenland (Harper et al., 2012). During our 2016 field campaign, colleagues from Ludwig Maximilian University, Munich, also investigated meltwater percolation at one of our study sites, using upwards-penetrating radar (Heilig et al., 2009; Mitterer et al., 2011) installed at a depth of ~4 m below the surface (Heilig et al., 2018). This provides a complementary dataset concerning the depth of meltwater penetration in summer, 2016.

Firn pits were excavated to depths of 2.2 and 5.3 m at two sites 650 m apart. Snow and firn density were measured at 10-cm intervals in the firn pits, using a 100-cm^3 box cutter. The 2015-2016 seasonal snowpack had a depth of ~0.9 m and was free of ice layers. The underlying firn was made up of a mixture of ice layers and porous firn, with the ice layers taking the form of discrete or continuous horizontal bands. Several ice layers were more than 10-cm thick. Figure 1 presents the ice-layer stratigraphy at each site, based on analysis of shallow firn cores drilled adjacent to the firn pits.

A chainsaw was used to cut through the thick ice layers and below about 2 m depth, where the firn became too dense for a shovel. The north-facing vertical face of each firn pit was instrumented with 8 thermistors and 8 time-domain reflectometry (TDR) probes to monitor snow water content. TDR measures bulk dielectric permittivity, ε_b, an excellent proxy for liquid water content in snow and firn (Denoth, 1984; Techel and Pielmeier, 2011). The relative dielectric permittivity of air, ice, and water are ε_a=1, ε_i ~3.2, and ε_w ~ 80. Because liquid water has such a high value compared to air and ice, the dielectric permittivity of snow increases strongly with liquid water content. Dielectric permittivity also increases with snow density, but water content is the main control on variations in ε_b (Stein et al., 1997; Schneebeli et al., 1998).

Installation depths for the thermistors and TDRs are indicated in Figure 1 and Table S1. Sensor spacing was irregular in order to concentrate observations near the surface as well as immediately above and below thick ice layers, to test whether these acted as impermeable barriers to water flow. The thermistors and TDR probes were wired to Campbell Scientific CR1000 dataloggers and data were recorded each 30 minutes from May 11 to September 30, 2016, capturing the complete melt season. Sensors were inserted horizontally into undisturbed snow and firn, with the probes extending 0.3 m into the wall of the firn pit. Pits were filled in with snow after the sensors were installed, several weeks in advance of the summer melt season.

An automatic weather station (AWS) configured for surface energy balance monitoring was also installed adjacent to site A. This pit was shared with the upward-looking radar experiments (Heilig et al., 2018). Sensors were left in place through the summer 2016 melt season and we returned to the sites in April 2017 to collect data and excavate the instruments. All data were quality-controlled and any missing data were gap-filled by linear interpolation.

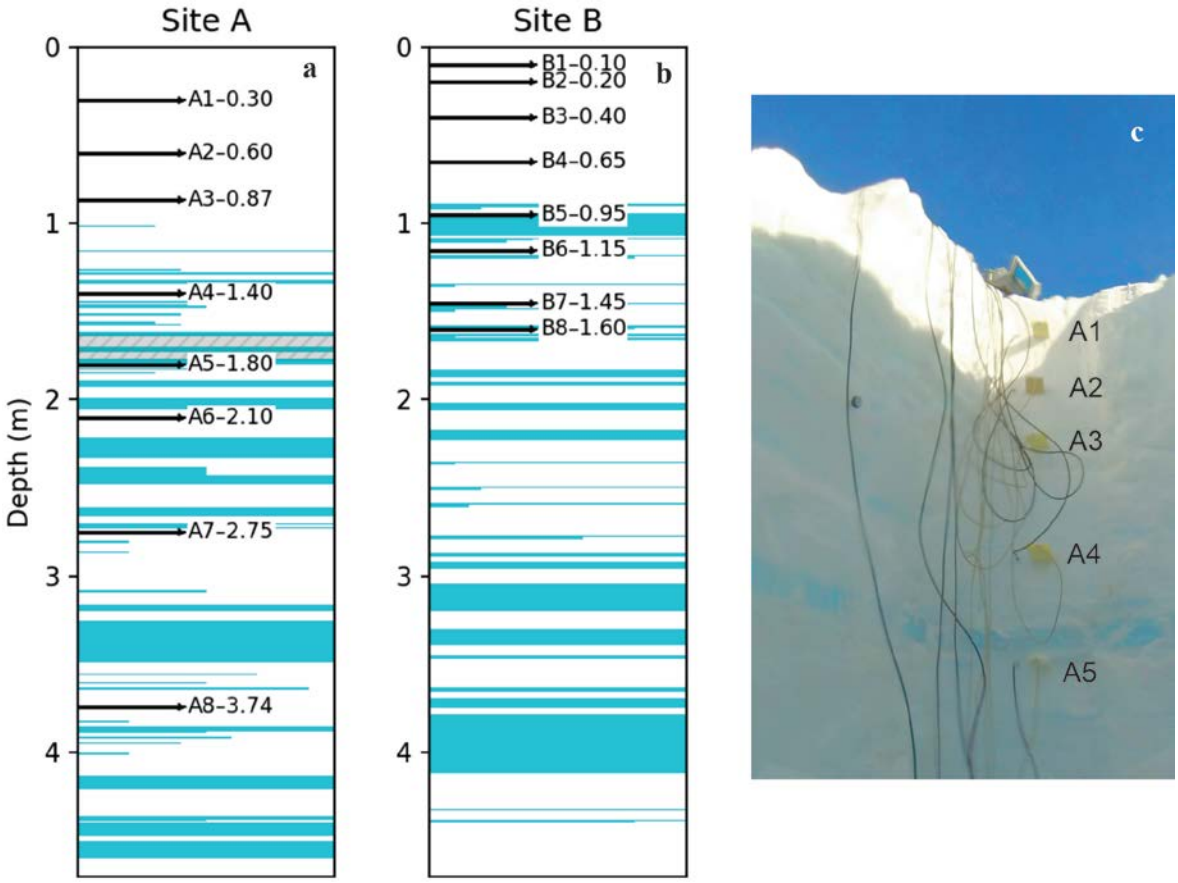

Figure 1. Ice-layer stratigraphy from sites a) A and b) B. Blue colors indicate ice layer location and thickness, and black arrows indicate the locations and depths (in m) of thermistors and TDR probes. The grey hatched zone in (a) highlights an 11-cm thick ice layer just above level A5 (1.68 to 1.79 m), as seen in photograph (c) of the upper ~2 m of pit A, which also shows thermistor/TDR installations A1 to A5. Photograph by Samira Samimi.

3 Results and Analysis

Figure S1 plots the evolution of air temperature, subsurface snow/firn temperature, and dielectric permittivy in the deep firn pit from May to September, 2016. At the time of sensor installation, near-surface firn was in the process of warming from the winter cold wave. Frequent daily maximum air temperatures above 0°C began in the first week of June, but it took ~two weeks for the snow at 0.3 m to warm to the melting point and for liquid water to be detected at that depth. Diurnal cycles of surface melting continued regularly into mid-August, accompanied by firn warming and meltwater infiltration to a depth of between 1.8 and 2.1 m. The depth of penetration of the wetting front coincided with the melting front (0°C isotherm). Sensors at and below 2.1 m depth remained frozen and dry. The summer melt season ended on August 26, with a return to persistent sub-zero air temperatures after this date.

Figures 2 and 3 examine the two main summer melt periods in each firn pit. The evolution of summer melting, snow/firn temperature, and dielectric permittivity was similar at the two sites, with evidence of thawing- and wetting-front propagation to similar depths. Site B offers more detail on the near-surface snowpack, with sensors at 0.1 and 0.2 m.

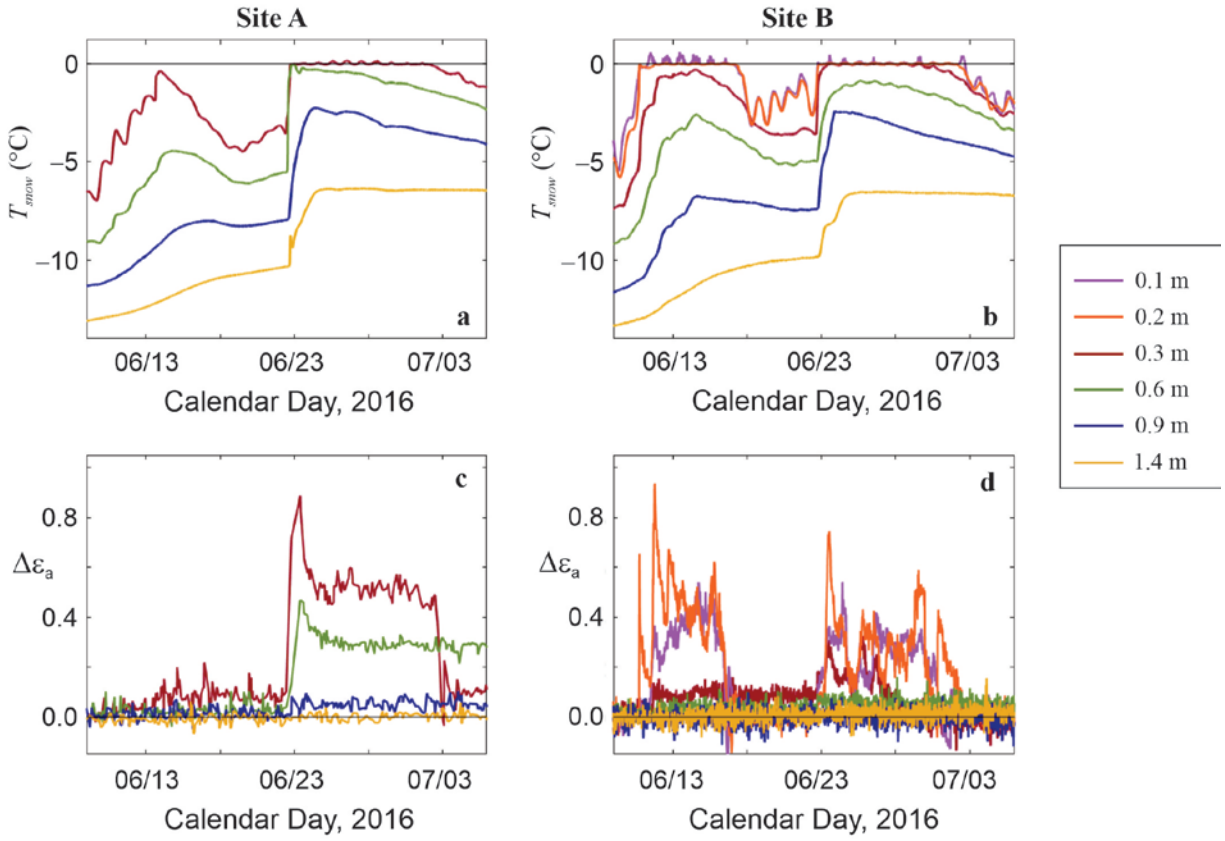

Figure 2. Observed (a,b) snow temperatures and (c,d) dielectric permittivity anomalies in the upper 1.4 m of firn pits A (left) and B (right) from June 9 to July 6, 2016, the onset of summer melt. The legend applies to all plots; values at 0.1 and 0.2 m were only measured at Site B.

Figure 2 presents the subsurface temperature and dielectric permittivity data during the period of melt onset at each site in the upper 1.4 m of each pit. Monitoring depths are not identical at sites A and B, but their nearest analogues are plotted, and are within 0.1 m of each other. The thermistor records from 0.3, 0.6, 0.9 and 1.4 m (Figures 2a,b) indicate the close agreement in snowpack thermal evolution at these two sites. Correlation coefficients for the summer temperature records at these two sites exceed 0.99 at these four depths.

Atmospheric warming in the first two weeks of June drove snowpack warming, with temperate conditions and surface melting evident at site B from June 11-16. The upper 0.2 m of the snowpack reached 0°C (Figure 2b), accompanied by increases in dielectric permittivity of ~0.4 to 0.9 (Figure 2d). Diurnal temperature peaks slightly greater than 0°C for the upper two

thermistors are likely due to absorption of solar radiation transmitted through the surface snow. The upper TDR sensor had a relatively constant liquid water content through this period, but the sensor at 0.2 m exhibited diurnal cycles. At and below 0.3 m, the snowpack remained frozen and dry at both sites through this initial phase of melting. Snow at 0.3 m depth at site A came close to the melting point on June 14, reaching –0.3°C before cooling again. Because of this, the summer melt onset was not detected at Site A.

Following a week of cooler temperatures, surface melting resumed on June 22 at both sites. This was marked by an abrupt subsurface warming, with the upper 0.6 m of snow becoming temperate and wet. Temperatures at 0.3 and 0.6 m at site A increased by 3.5 and 5.4°C over a six-hour period, both reaching 0°C (Figure 2a). The sensor at 0.9 m depth also recorded a warming of 5.5°C, but over 32 hours, with an abrupt step followed by continued warming at a slower rate. Deeper thermistors also registered this step warming, but firn below ~0.6 m depth remained dry, with temperatures below the melting point. In the upper 0.3 m at both sites, conditions remained temperate and wet until July 2, at which point another cooling cycle forced a return to cold, dry conditions.

The summer melt season resumed on July 19, with a sustained period of warm temperatures, melting conditions, and meltwater penetration to depth (Figure 3). This was characterized by a second abrupt warming event in the upper 1.4 m, registered by the top five thermistors at site A and all thermistors at site B (Figures 3a,b). Dielectric permittivities rose sharply at these depths, coincident with temperatures reaching 0°C (Figures 3c,d), although the increase in ε_b was less for the deeper sensors. The upper two sensors at site B, at 0.1 and 0.2 m, experienced more meltwater than underlying sites in either pit, with $\Delta\varepsilon_b$ values greater than 2 (Figure 3d). The abrupt onset of temperate, wet conditions in the upper snow and firn was followed by a more gradual warming below this, recorded at the sensors from 1.8 to 3.7 m depth (Figures S1b and 3a). The wetting front and the 0°C isotherm reached 1.8 m depth by August 12, but firn below this remained sub-zero and dry.

Atmospheric cooling in mid-August caused the near-surface snowpack (upper 0.3 m) to refreeze ($\varepsilon_b \sim \varepsilon_{b0}$), but there was a temperate layer from about 0.6 m to 1.4 m, sandwiched between sub-zero conditions above and below (Figures 3a,b). This was most strongly evident at 0.9 m, where wet-snow conditions persisted until August 22 at both sites. These middle layers of the firn pits were the last to refreeze, as latent heat of refreezing meltwater maintained temperate conditions at these depths for several days before seasonal cooling ensued.

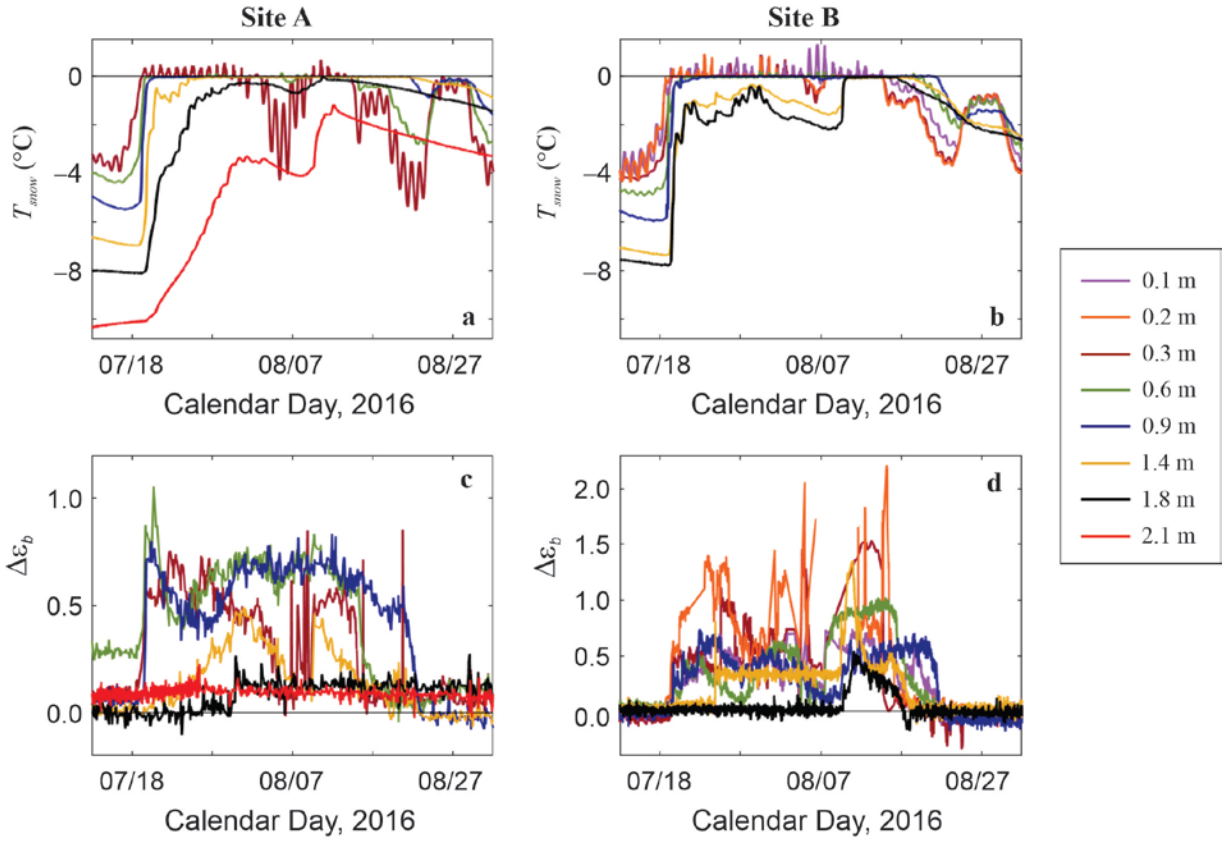

Figure 3. Observed (a,b) snow temperatures and (c,d) dielectric permittivity anomalies in the upper 2.1 m of firn pits A (left side) and B (right side) for the main summer melt season from July 13 to September 1, 2016. The legend applies to all plots; values at 0.1 and 0.2 m were only measured at Site B and 2.1 m is only at site A. Note the different scale in plots (c) and (d).

There is no indication of meltwater percolation below the surface at either site after August 22. Air temperatures above 0°C afrom Aug 23-25 warmed the upper snowpack at both sites, with some lag, but ε_b remained at background levels (Figure 3). This is the only time through the summer when temperate snow conditions were not accompanied by evidence of liquid water. Net energy at the surface was negative at this time and there may have been meltwater refreezing at the surface, above the upper TDR probes. Latent heat generated near the surface may have conductively warmed the underlying snow, but without meltwater infiltration.

Meltwater successfully percolated through several ice layers in the upper meter of firn at both sites. There were no ice layers in the winter snowpack, representing the upper ~0.9 m, but the underlying firn contained several discrete ice layers, some thin (1 mm to 2 cm), and others substantial. This included an 11-cm thick ice layer from 1.68 to 1.79 m depth at Site A and a 12-cm thick ice layer from 0.95 to 1.07 m depth at site B (Figure 1). In total over the upper 1.8 m, we measured 22 cm of ice in 11 discrete layers at site A and 19 cm of ice in 9 discrete layers at site B. Meltwater effectively penetrated through all of these ice layers, although not until temperatures reached the melting point at these depths. This implies that ice layers became permeable when they transitioned to a temperate state.

4 Discussion

The thermistor and TDR data give a consistent account of the thermal evolution and meltwater infiltration at Dye 2 site in summer, 2016. The melting front, characterized by 0°C conditions and evidence of liquid water, penetrated to a depth of between 1.8 and 2.1 m. Below this, temperatures remained less than 0°C, there were no abrupt warming events, and dielectric permittivities did not rise above their background levels. This is consistent with observations from the upward-looking radar at site A, which also indicate only shallow penetration of the wetting front into the firn in summer 2016 (Heilig et al., 2018).

To our knowledge, these data represent the first direct observations of meltwater penetration through ice layers in the Greenland percolation zone. This result implies thermodynamic controls on the depth of meltwater infiltration, rather than impermeability limits imposed by ice layers. We were not present in the summer melt season to directly observe this, but it may be that ice layers become soft or slushy. Overall, the depth of the melting front (the 0°C isotherm) appears to have been the main barrier to deep penetration of meltwater during summer 2016.

Whether ice layers can be altered to become permeable depends on the thermal energy available for warming the firn and maintaining temperate conditions. Warming occurs through a combination of thermal conduction, driven by summer atmospheric warming, latent heat release from meltwater refreezing, and advective heat transfer associated with meltwater penetration into sub-zero snow. These mechanisms are very clear in the thermistor data, with gradual temperature shifts in response to atmospheric warming and cooling trends punctuated by three abrupt warming events, reaching progressively deeper into the snow and firn (Figures 2 and 3). The latter are too rapid to be due to thermal conduction, so must be associated with meltwater advection and refreezing. Meltwater penetration to depth appears to follow a stepped process, facilitated by latent heat release.

Ultrasonic depth gauges installed adjacent to each firn pit recorded a total ablation of ~0.35 m over the summer. This was partially offset by several periods of snowfall, with a total summer accumulation of about 0.25 m. Most of the measured surface lowering occurred from July 18 to August 10, in line with the main melt season (Figure 3). Based on our density measurements, we estimate a total summer melt of 160 mm w.e. All of this meltwater likely refroze within the upper 1.8 m of the snow and firn, with an associated latent heat release of 5.3×10^7 J m^{-2}. Distributed over the 1.8-m snow/firn column with an average density of 480 kg m^{-3}, this energy would warm the firn by 14.8°C. This indicates that latent heat release was sufficient to drive the warming to temperate conditions over 1.8 m depth, although conductive heat flux also played an important role in the early melt season.

The observations provide new insight into meltwater percolation and refreezing processes in the percolation zone of the Greenland Ice Sheet. In particular, we present clear evidence of meltwater penetration through ice layers and thermodynamic controls on meltwater percolation depth. Ice layers appear to become permeable when warmed to 0°C, which would promote meltwater retention in firn. We saw no evidence of meltwater penetration through frozen (sub-zero) ice layers; these are likely to present impermeable barriers, as is commonly assumed (*e.g.*,

Machguth et al., 2016; Noël et al., 2017; MacFerrin et al., 2019). As such, ice layers may still present an effective barrier to meltwater percolation where they are extensive (with a high thermal inertia) or when there is insufficient thermal energy to thaw such layers. Where there are thick ice slabs, such as in the lower percolation zone (MacFerrin et al., 2019; Vandecrux et al., 2019), high quantities of seasonal meltwater can provide large amounts of latent heat to thaw near-surface snow, firn, and ice layers, but there must be sufficient pore space where meltwater can refreeze. Impermeable ice layers close to the surface would limit this process. In addition, refreezing will desist once near-surface snow and firn are temperate, eliminating latent heat as a mechanism for firn warming. Thick near-surface ice slabs are therefore less likely to reach a temperate, permeable state, especially when insufficient snow and firn are present above them to store substantial quantities of meltwater.

The summer evolution of snow-water content is consistent with propagation of a wetting front that tracks the 0°C isotherm in the snow and firn, rather than episodic drainage through preferential flow. We conclude this based on the near-simultaneous arrival of the wetting front at our two sites, and its progressive propagation to depth over the course of the melt season. The measurements only represent two points, however, and preferential flow paths or 'piping' may well be the dominant mechanism of meltwater infiltration in firn (Humphrey et al., 2012; Wever et al., 2016). We also cannot rule out meltwater penetration to depths greater than 2 m at other locations in the Dye 2 region in summer 2016. Spatial variability is a large challenge in understanding and modelling firn hydrology and meltwater retention in Greenland. Our measurements nevertheless provide helpful insights to modelling efforts of meltwater infiltration into firn (*e.g.*, Wever et al., 2016; Steger et al., 2017), in particular the observation that ice layers do not always act as impermeable barriers to flow. Additional measurements like those reported here, especially during melt seasons of variable intensity, could help to track meltwater penetration into firn in the lower percolation zone and other sectors of Greenland.

Uncertainties

Sensor depths are reported as constant values in this manuscript, but actual depths changed over the course of the study, in association with fresh snowfall and surface ablation. All instruments at site A were deep enough to avoid melt-out. However, ablation from July 18 to August 10 was sufficient to expose the uppermost (0.1 m) sensors at site B, and inspection of the data is consistent with melt-out at this level on August 5. A ~0.15 m snow event from August 10 to 12 buried the melted-out sensors and they give sensible signals again after this point.

With our study setup, there is a risk that water flows or percolates more easily into the disturbed area of the firn pits, but we see no evidence of this. The thermal and hydrological evolution appear to be natural, are virtually identical at the two sites, and only extend to a limited depth in the pits with each abrupt event. As the pits were excavated to below the lower-most sensors, free-flowing water in the disturbed areas would be expected to propagate deeper. The low rates of meltwater production and low-sloping environment at Dye 2 are more conducive to vertical infiltration than lateral flows, and the data are consistent with that expectation. We are therefore confident that the thermodynamic and hydrological signals reflect vertical meltwater infiltration from above, without influence from the disturbed snow in the firn pit.

5 Conclusions

The thermistor, TDR, and AWS data provide a consistent and detailed account of the coupled thermodynamic and hydrological processes governing meltwater percolation and refreezing at Dye 2. This dataset presents an excellent opportunity to constrain the effective thermal and hydraulic conductivities of polar snow and firn, to help constrain models of firn hydrology. Modelling of the joint thermal and hydrological evolution of the near-surface firn will be examined in follow-up work. Additional measurements are needed to test and confirm the inferred processes at other locations in Greenland's percolation zone.

Measurements from the two sites 650 m apart are exceptionally coherent, and indicate that meltwater at Dye 2 percolated to a depth of about 2 m in summer 2016. The wetting front and the melting front were coincident at the two sites, implying thermodynamic controls on meltwater infiltration. Meltwater penetrated through ice layers up to 12 cm thick, but there is no evidence of meltwater infiltration through ice layers until firn temperatures reached 0°C. We hypothesize that melting conditions may have turned the ice layers into more permeable, slush-like horizons. The depth of the 0°C isotherm, rather than the presence of ice layers, governed firn permeability and meltwater penetration depth at our sites. This observation is a significant advancement in understanding meltwater infiltration and retention in polar firn. For an ice layer to become permeable, sufficient latent heat release is needed in the overlying firn and snow, which depends on the available pore space, cold content, and meltwater supply. Ice slabs that are thick or close to the surface may be difficult to thaw, as heat transfer will be dramatically reduced once firn is temperate or saturated. Models of this process can help to project whether meltwater is likely to infiltrate vertically or be redirected laterally, contributing to ice sheet runoff.

Acknowledgements

We thank Baptiste Vandecrux, Darren Hill, Achim Heilig, Bastian Gerling, and Leander Gambal for support with the field work. The U.S. National Science Foundation, Air National Guard, and CH2MHill Polar Field Services provided essential logistical support for this field work. Research costs of SS and SJM were supported by the Natural Sciences and Engineering Research Council (NSERC) of Canada, and funding for MM and the FirnCover project was from NASA Award NNX15AC62G. Data from this study will be available at the U.S. National Snow and Ice Data Centre. The authors declare no conflicts of interests with the conclusions of this study.

References

Denoth, A. (1994). An electronic device for long-term snow wetness recording. *Annals of Glaciology*, *19* (1), 104-106, https://doi.org/10.3189/S0260305500011058.

Forster, R. R., Box, J. E., van den Broeke, M. R., Miège, C., Burgess, E. W., Van Angelen, J. H., et al. (2014). Extensive liquid meltwater storage in firn within the Greenland ice sheet. *Nature Geoscience*, *7* (2), 95-98, https://doi.org/10.1038/ngeo2043.

Harper, J., Humphrey, N., Pfeffer, W. T., Brown, J., & Fettweis, X. (2012). Greenland ice-sheet contribution to sea-level rise buffered by meltwater storage in firn. *Nature*, *491*, 240–243, doi: 10.1038/nature11566.

Humphrey, N. F., Harper, J. T., & Pfeffer, W. T. (2012). Thermal tracking of meltwater retention in Greenland's accumulation area. *Journal of Geophysical Research*, *117*, F01010. https://doi.org/10.1029/2011JF002083.

Heilig, A., M. Schneebeli, & Eisen, O. (2009). Upward-looking ground-penetrating radar for monitoring snowpack stratigraphy, *Cold Regions Science and Technology*, *59* (2–3), 152–162, doi:10.1016/j.coldregions.2009.07.008.

Koenig, L. S., Miège, C., Forster, R. R., & Brucker, L. (2014). Initial in situ measurements of perennial meltwater storage in the Greenland firn aquifer. *Geophysical Research Letters*, *41* (1), 81-85, https://doi.org/10.1002/2013GL058083.

MacFerrin, M., Machguth, H., van As, D., Charalampidis, C., Stevens, C. M., A. Heilig, A., et al. (2019). Rapid expansion of Greenland's low-permeability ice slabs. *Nature*, 573, 403-407, doi:10.1038/s41586-019-1550-3.

Marks, D., & Dozier, J. (1992). Climate and energy exchange at the snow surface in the Alpine region of the Sierra Nevada: 2. Snow cover energy balance. *Water Resources Research*, *28*, 3043–3054, https://doi.org/10.1029/92WR01483.

Mitterer, C., Heilig, A., Schweizer, J., & Eisen, O. (2011). Upward-looking ground-penetrating radar for measuring wet-snow properties. *Cold Regions Science and Technology*, *69* (2–3), 129–138, https://doi.org/10.1016/j.coldregions.2011.06.003.

Mouginot, J., Rignot, E., Bjørk, A. A., van den Broeke, M., Millan, R., Morlighem, M., et al. (2019). Forty-six years of Greenland Ice Sheet mass balance from 1972 to 2018. *Proceedings of the U.S. National Academy of Sciences*, *116* (19), 9239-9244, https://doi.org/10.1073/pnas.1904242116.

Noël, B., van de Berg, W. J., Lhermitte, S., Wouters, B., Machguth, H., Howat, I., et al. (2017). A tipping point in refreezing accelerates mass loss of Greenland's glaciers and ice caps. *Nature Communications*, *8* (1), 1-8, doi:10.1038/ncomms14730.

Pfeffer, W. T., M. F. Meier, & Illangasekare, T. H. (1991). Retention of Greenland runoff by refreezing: Implications for projected future sea level change, *Journal of Geophysical Research*, *96* (C12), 22117–22124, doi:10.1029/91JC02502.

Pfeffer, W. T., & Humphrey, N. F. (1998). Formation of ice layers by infiltration and refreezing of meltwater. *Annals of Glaciology*, *26*, 83-91, https://doi.org/10.3189/*1998AoG26*-1-*83-91*.

Rennermalm, A. K., Moustafa, S. E., Mioduszewski, J., Chu, V. W., Forster, R. R., Hagedorn, B., et al. (2013). Understanding Greenland ice sheet hydrology using an integrated multi-scale approach. *Environmental Research Letters*, *8* (1), 015017, doi: 10.1088/1748-9326/8/1/015017.

Samimi, S., & Marshall, S. J. (2017). Diurnal cycles of meltwater percolation, refreezing, and drainage in the supraglacial snowpack of Haig glacier, Canadian Rocky Mountains. *Frontiers in Earth Science*, *5*, 6, https://doi.org/10.3389/feart.2017.00006.

Schneebeli, M., Coléou, C., Touvier, F. & Lesaffre, B. (1998). Measurement of density and wetness in snow using time-domain reflectometry. *Annals of Glaciol*ogy, *26*, 69-72, https://doi.org/10.3189/*1998AoG26*-1-*69-72*.

Steger, C. R., Reijmer, C. H., van den Broeke, M. R., Wever, N., Forster, R. R., Koenig, L. S., et al. (2017). Firn meltwater retention on the Greenland Ice Sheet: a model comparison. *Frontiers in Earth Science*, *5* (3), https://doi.org/10.3389/feart.2017.00003.

Stein, J., Laberge, G., & Lévesque, D. (1997). Monitoring the dry density and the liquid water content of snow using time domain reflectometry (TDR). *Cold Regions Science and Technology*, *25* (2), 123-136, doi:10.1016/S0165-232X(96)00022-5.

Techel, F., & Pielmeier, C. (2011). Point observations of liquid water content in wet snow – investigating methodical, spatial and temporal aspects. *The Cryosphere*, *5*, 405-418, doi:10.5194/tc-5-405-2011.

van As, D., Box, J. E., & Fausto, R. S. (2016). Challenges of quantifying meltwater retention in snow and firn: an expert elicitation. *Frontiers in Earth Science*, *4* (101), https://doi.org/10.3389/feart.2016.00101.

Vandecrux, B., MacFerrin, M., Machguth, H., Colgan, W. T., van As, D., Heilig, A., et al. (2019). Firn data compilation reveals widespread decrease of firn air content in western Greenland. *The Cryosphere*, 13, 845–859, https://doi.org/10.5194/tc-13-845-2019.

Verjans, V., Leeson, A. A., Stevens, C. M., MacFerrin, M., Noël, B., & van den Broeke, M. R. (2019). Development of physically-based liquid water schemes for Greenland firn-densification models. *The Cryosphere*, 13, 1819-1842, https://doi.org/10.5194/tc-13-1819-2019.

Vernon, C. L., Bamber, J. L., Box, J. E., van den Broeke, M. R., Fettweis, X., Hanna, E., & Huybrechts, P. (2013). Surface mass balance model intercomparison for the Greenland ice sheet. *The Cryosphere*, *7*, 599–614, https://doi.org/10.5194/tc-7-599-2013.

Wever, N., Würzer, S., Fierz, C., & Lehning, M. (2016). Simulating ice layer formation under the presence of preferential flow in layered snowpacks. *The Cryosphere*, *10*, 2731–2744, https://doi.org/10.5194/tc-10-2731-2016.

Meltwater Penetration Through Temperate Ice Layers in the Percolation Zone at DYE-2, Greenland Ice Sheet

Samira Samimi[1], Shawn J. Marshall[1,2] and Michael MacFerrin[3]

[1] Department of Geography, University of Calgary, Calgary, Alberta, Canada
[2] Environment and Climate Change Canada, Gatineau, Quebec, Canada
[3] Cooperative Institute for Research in Environmental Sciences, University of Colorado, USA

Corresponding author: Samira Samimi (samira.samimi@ucalgary.ca)

Key Points:

- Time-domain reflectometry probes give direct measurements of meltwater infiltration in firn at DYE-2 on the southwest Greenland Ice Sheet.
- We document meltwater penetration through ice layers up to 12 cm thick in temperate firn.
- The wetting front and melting front developed in tandem, indicating coupled hydrological and thermodynamic controls on meltwater infiltration depth.

Abstract

Meltwater retention in the firn layer of the Greenland Ice Sheet has the potential to buffer sea level rise due to ice sheet melt. The capacity of the firn layer to store meltwater is unclear, however, because refrozen ice layers can act as impermeable barriers to meltwater percolation, promoting runoff rather than retention. We present time-domain reflectometry and thermistor data which demonstrate that meltwater successfully penetrates ice layers up to 12 cm thick in the near-surface firn at DYE-2, Greenland. Our observations indicate that ice layers within polar firn can be permeable when summer warming and latent heat release from meltwater refreezing raise firn temperatures to the melting point. The extent and depth of refreezing, as determined by the coupled thermodynamic and hydrological evolution in the firn, are more important than the presence of ice layers in governing meltwater infiltration and retention at our study site.

Plain Language Summary

Meltwater that percolates below the surface of the Greenland Ice Sheet is difficult to track; some of it contributes to runoff, mass loss, and sea level rise, but some meltwater refreezes and is retained within the system. Greenland has a large firn area, where multi-year snow that has not yet transitioned to glacial ice has pore space that can retain meltwater. To improve understanding of hydrological and mass balance processes in polar firn, we excavated two firn pits in the Greenland Ice Sheet accumulation area in spring, 2016, and instrumented these pits with thermistors and time-domain reflectometry (TDR) sensors, connected to continuously-recording dataloggers. These sensors allowed us to directly track the coupled thermal and hydrological evolution in the firn through the summer melt season. We recorded nearly identical conditions at each site, with evidence of meltwater infiltration to a depth of between 1.8 m and 2.1 m and a wetting front that was thermally controlled, i.e. coincided with the melting front. This included meltwater penetration through numerous ice layers, including layers up to 12 cm thick. All of this meltwater refroze. Our results indicate that ice layers do not necessarily act as impermeable barriers to meltwater percolation and retention.

1 Introduction

Mass loss from the Greenland Ice Sheet has increased in recent decades due to significant increases in meltwater runoff (van den Broeke et al., 2009; Bamber et al., 2018; Mouginot et al., 2019). One of the challenges in estimating the current and future contribution of the ice sheet to sea level rise is the fact that surface melting does not always lead to runoff. In the percolation zone, meltwater that infiltrates the underlying cold snow or firn can be retained as liquid water (Forster et al., 2014; Koenig et al., 2014) or as refrozen ice (Pfeffer et al., 1991; Pfeffer and Humphrey, 1998; Harper et al., 2012). This reduces summer runoff and ice sheet contributions to sea level rise (Harper et al., 2012; Rennerhalm et al., 2013). Meltwater retention processes may be increasingly important as melting propagates to higher elevations in Greenland in a warming world (Vernon et al., 2013).

Meltwater that percolates and refreezes is difficult to account for in altimetric measurements of surface mass balance, as it is not possible to detect how much meltwater is retained within the system. This is also a source of uncertainty in mass balance models, as processes of meltwater percolation and refreezing occur at fine scales, are spatially heterogeneous, and *in situ* observations are scarce (*e.g.*, Harper et al., 2012; van As et al., 2016; Verjans et al., 2019, Vandecrux et al, 2019). This makes it difficult to calibrate and validate models of these processes, particularly on the scale of polar ice caps and ice sheets.

The extent to which meltwater retention in firn can buffer mass loss and sea-level rise is also unclear. Greenland's firn zone covers about 80% of the ice sheet, but refrozen near-surface ice layers have the potential to act as impermeable barriers, redirecting meltwater percolation into runoff (Gascon et al., 2013; Noel et al., 2017; MacFerrin et al., 2019; Ashmore et al., 2020). In the percolation zone, firn densification associated with warming and refreezing is also leading to a loss of available pore space, imposing further limits on meltwater storage capacity as melting progresses inland (Vandecrux et al., 2019). These processes can increase the ratio of meltwater runoff to retention. Hence, models of meltwater infiltration also need to account for ice-layer and firn-densification processes. These represent significant uncertainties in projections of the Greenland ice sheet's response to climate warming.

To examine meltwater infiltration and refreezing processes in the Greenland ice sheet percolation zone, we instrumented two firn pits with arrays of thermistors and time-domain reflectometry (TDR) sensors in order to track the coupled thermal and hydrological evolution in the seasonal snow and the upper ~3 m of firn through a summer melt season. The TDR sensors provide continuous measurements of dielectric permittivity, a proxy for liquid water content in the snow and firn. This manuscript presents these *in situ* observations and their implications for meltwater retention in firn. The experiment builds on Humphrey et al. (2012), who used thermistor arrays to track the thermal signature of meltwater infiltration in firn, which is apparent through the latent heat release when meltwater refreezes. Through the addition of TDR probes, we directly trace meltwater flow in the near-surface snow and firn. A similar experimental setup in the Canadian Rocky Mountains successfully demonstrated the ability to track meltwater percolation, refreezing, and snow-water content in a supraglacial snowpack using TDR probes (Samimi and Marshall, 2017). The implementation in Greenland extends these methods to polar firn, where liquid water content is lower and meltwater refreezing is more significant.

2 Methods

Measurements were established in May, 2016 in two firn pits near DYE-2 station in southwestern Greenland (see Figure S1 in the Supporting Information). The study sites, denoted A and B, were at an elevation of 2120 m, representing the upper percolation zone in southern Greenland (Harper et al., 2012). Co-ordinates of each firn pit are included in Table S1. During our 2016 field campaign, colleagues from Ludwig Maximilian University, Munich, also investigated meltwater percolation at site A, using upward-penetrating radar installed at a depth of ~4 m below the surface (Heilig et al., 2018). This provides a complementary dataset concerning the depth of meltwater penetration in summer 2016.

Firn pits were excavated to depths of 5.3 m at Site A and 2.2 m at Site B. The pits were located 400 m apart (Figure S1), with Site B included to provide a sample of the spatial variability of meltwater infiltration under similar climatic and snow/firn conditions. Measurements were also concentrated closer to the surface at Site B (Figure 1). Snow and firn density were measured at 10-cm intervals in the firn pits, using a 100-cm^3 box cutter. Density values at the depths of sensor installatons are reported in Table S1. The 2015-2016 seasonal snowpack had a depth of ~0.9 m and was free of ice layers. The underlying firn was made up of a mixture of ice layers and porous firn, with numerous ice layers in the form of discrete or continuous horizontal bands. Several ice layers were more than 10-cm thick. Figure 1 presents the ice-layer stratigraphy at each site, based on analysis of firn cores drilled about 3 m from each firn pit. The firn cores provide higher-quality stratigraphic records, permitting accurate characterization of ice layer thickness and extent. Firn exhibits considerable small-scale heterogeneity in the location and thickness of ice layers, so the firn core stratigraphy differs from that of the pits. However, the total ice content and the number and thickness of ice layers were similar in the fire cores and in the pits, including the presence of thick ice layers (>10 cm) in the upper 2 m of firn (e.g., Figure 1c). We therefore consider the ice-layer stratigraphy in Figure 1 to be representative.

A chainsaw was used to cut through the thick ice layers and below ~2 m depth, where the firn became too dense for a shovel. The north-facing vertical face of each firn pit was instrumented with 8 thermistors and 8 time-domain reflectometry (TDR) probes to monitor snow water content. TDR measures bulk dielectric permittivity, ε_b, an excellent proxy for liquid water content in snow and firn (Denoth, 1994; Techel and Pielmeier, 2011). The relative dielectric permittivity of air, ice, and water are ε_a=1, $\varepsilon_i \sim 3.2$, and $\varepsilon_w \sim 80$. Because liquid water has such a high value compared to air and ice, the dielectric permittivity of snow increases strongly with liquid water content. Dielectric permittivity also increases with snow density, but water content is the main control on variations in ε_b (Stein et al., 1997; Schneebeli et al., 1998).

Installation depths for the thermistors and TDRs are indicated in Figure 1 and Table S1. Sensors were installed in pairs at 8 different depths in each pit, with thermistor and TDR probes inserted about 15 cm apart at each depth. Sensors were inserted horizontally into undisturbed snow and firn, with the probes extending 0.3 m into the wall of the firn pit. Sensor spacing with depth was irregular in order to concentrate observations near the surface as well as immediately above and below thick ice layers, to test whether these acted as impermeable barriers to water flow. Pits were filled in with snow after the sensors were installed, several weeks in advance of the summer melt season. The thermistors and TDR probes were wired to Campbell Scientific CR1000 dataloggers and data were recorded every 30 minutes from May 11 to October 28, 2016.

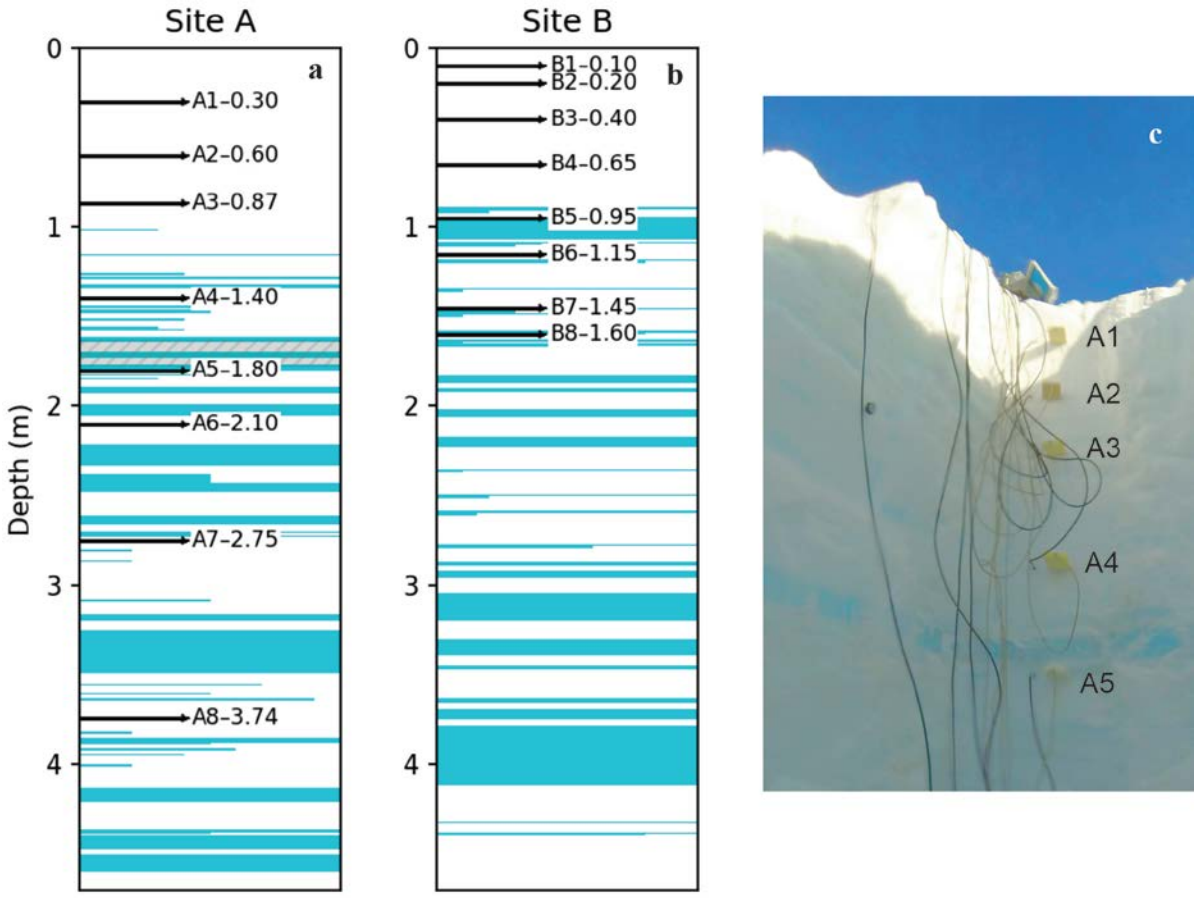

Figure 1. Ice-layer stratigraphy from sites a) A and b) B. Blue colors indicate ice layer location and thickness, and black arrows indicate the locations and depths (in m) of thermistors and TDR probes. The grey hatched zone in (a) highlights an 11-cm thick ice layer just above level A5 (1.68 to 1.79 m), as seen in photograph (c) of the upper ~2 m of pit A. The photograph also shows thermistor/TDR installations A1 to A5. Photograph by Samira Samimi.

We returned to the site in April 2017 to collect data and excavate the instruments. An automatic weather station (AWS) configured for surface energy balance monitoring was also installed adjacent to site A. Details on the AWS instrumentation and data processing are provided in the Supporting Information. All data were quality-controlled, and missing TDR data were gap-filled by linear interpolation. AWS data were used to calculate the surface energy fluxes and meltwater production over the summer, using the surface energy balance model of Ebrahimi and Marshall (2016) combined with a 1D subsurface model of the coupled thermal and hydrological evolution in the upper 10 m of snow and firn. The subsurface model considers thermal diffusion, advective heat transport from meltwater advection, and latent heat release from meltwater refreezing, combined with a simple model of meltwater percolation (Samimi and Marshall, 2017). The Supporting Information discusses the energy balance and subsurface models in detail.

3 Results and Analysis

The summer 2016 melt season ran from the second week of June until late August, with the main period of melt from July 18 to August 9. Details of the AWS data, the modeled surface melt and energy fluxes, and the complete subsurface TDR and thermistor datasets are presented in the Supporting Information (Figures S2 and S3).

Figure 2 presents the observed air temperature, melt rates, and subsurface temperature and dielectric permittivity during the period of melt onset in the upper 1.4 m of each firn pit. Melt is calculated from the surface energy balance in the upper snow layer (0.1 m), and can occur when air temperature is below 0°C if surface snow/firn is at the melting point and net energy is positive. Dielectric permittivities are plotted as anomalies relative to the initial (dry) values at each site. Monitoring depths are not identical at sites A and B, but their nearest analogues are plotted in Figure 2, and are within 0.1 m of each other. Site B offers more resolution of the near-surface snowpack, with sensors at 0.1 and 0.2 m. The thermistor records from 0.3, 0.6, 0.9 and 1.4 m (Figures 2c,d) indicate the close agreement in snow/firn thermal evolution at these two sites. Correlation coefficients for the two sites exceed 0.99 at these four depths.

Atmospheric warming in the first two weeks of June drove snowpack warming, with surface melting beginning on June 5 and temperate conditions first evident at site B from June 11-16. The upper 0.2 m of the snowpack warmed abruptly to 0°C (Figure 2d), accompanied by increases in dielectric permittivity of ~0.4 to 0.9 (Figure 2f). Diurnal temperature peaks slightly greater than 0°C for the upper two thermistors are likely due to absorption of solar radiation transmitted through the surface snow. At and below 0.3 m, the snowpack remained frozen and dry at both sites through this initial phase of melting. Snow at 0.3 m depth at site A came close to the melting point on June 14, reaching –0.3°C before cooling again (Figure 2c). Because the initial pulse of melting and refreezing was confined to the upper 0.2 m of the snowpack, the summer melt onset was not detected at site A.

A second melt event followed a week of cooler temperatures (Figure 2a) and was marked by an abrupt subsurface warming on June 23, with the upper 0.6 m of snow becoming temperate and wet at both sites. Over a six-hour period, temperatures at 0.3 and 0.6 m at site A increased by 3.5 and 5.4°C, respectively, both reaching 0°C (Figure 2c). Deeper thermistors also registered this abrupt warming (e.g., +5.5°C over 32 hours at 0.9 m), but firn below ~0.6 m depth remained frozen and dry. Temperate and wet conditions persisted in the upper 0.3 m until July 2, at which point another cooling cycle forced a return to cold, dry conditions at both sites. All of the meltwater within the system appears to have refrozen at this time.

The summer melt season resumed on July 19, with a sustained period of melting conditions and meltwater penetration to 1.4 m depth (Figure 3). This was characterized by a third abrupt warming event, registered by the top five thermistors at site A and all thermistors at site B (Figures 3c,d). Dielectric permittivities rose sharply at these depths, coincident with temperatures reaching 0°C (Figures 3e,f), although the increase in ε_b was less for the deeper sensors. The upper two sensors at site B experienced more meltwater than underlying sites in either pit, with $\Delta\varepsilon_b$ values of up to 2 (Figure 3f). The abrupt onset of temperate, wet conditions in the upper snow and firn was followed by a more gradual warming below this, recorded at the sensors from

1.8 to 3.7 m depth (Figures 3c and S2b). The wetting front and the 0°C isotherm reached 1.8 m depth by August 12, but firn below this remained frozen and dry.

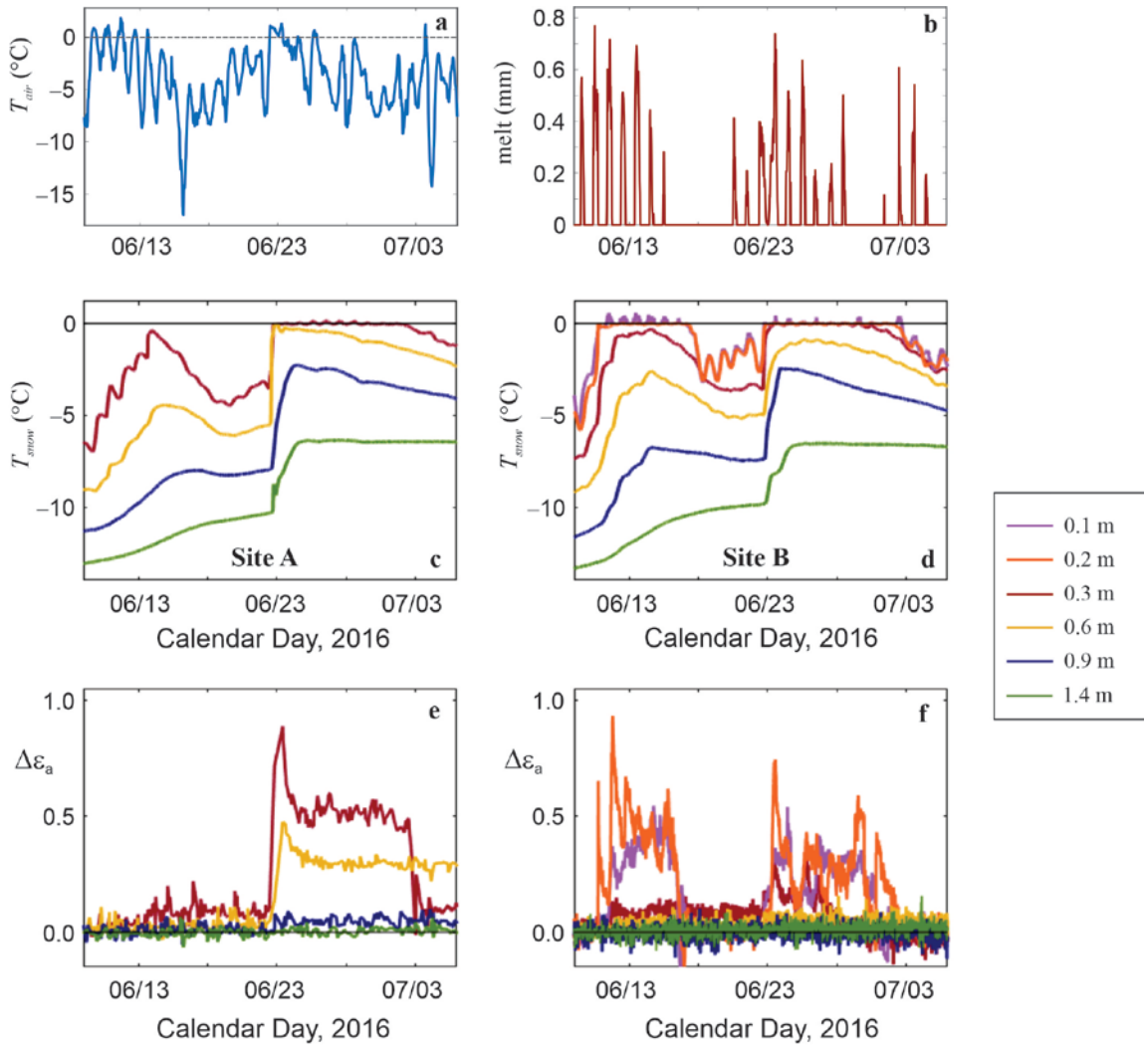

Figure 2. Observations during the onset of summer melt, June 9 to July 6, 2016: (a) air temperature, (b) modelled 30-minute melt (mm w.e.), (c,d) snow temperatures and (e,f) dielectric permittivity anomalies. Data in (c) to (f) are for the upper 1.4 m of firn pits A (left) and B (right). The legend applies to plots (c) to (f); values at 0.1 and 0.2 m were only measured at Site B.

Atmospheric cooling in mid-August (Figure 3a) caused the upper 0.3 m of the snowpack to refreeze ($\varepsilon_b \sim \varepsilon_{b0}$), but there was a temperate layer from about 0.6 m to 1.4 m, sandwiched between sub-zero conditions above and below (Figures 3c,d). This was most strongly evident at 0.9 m, where temperate, wet conditions persisted until August 22 at both sites. These middle layers of the firn pits were the last to refreeze, as latent heat of refreezing meltwater maintained temperate conditions at these depths for several days before seasonal cooling ensued.

There is no indication of meltwater percolation below the surface after August 22. Low rates of melting continued for several more days until shutting down for the summer on August 28, with an average melt rate of 2.9 mm w.e. d^{-1} from August 23-28. The upper snowpack warmed at both sites during these days, but ε_b remained at background levels. This is the only time over the summer when temperate snow conditions were not accompanied by evidence of liquid water. This melt event came following an atmospheric cooling cycle (Figure 3a) which caused the upper 0.3 m of the snowpack to refreeze and drop to temperatures of –2 to –5°C (Figure 3c,d). Combined with the low melt rates, the cold content of the snow appears to have been sufficient for meltwater to refreeze near the surface, above the upper TDR probes. Latent heat generated by the near-surface refreezing may have conductively warmed the underlying snow, but without meltwater infiltration.

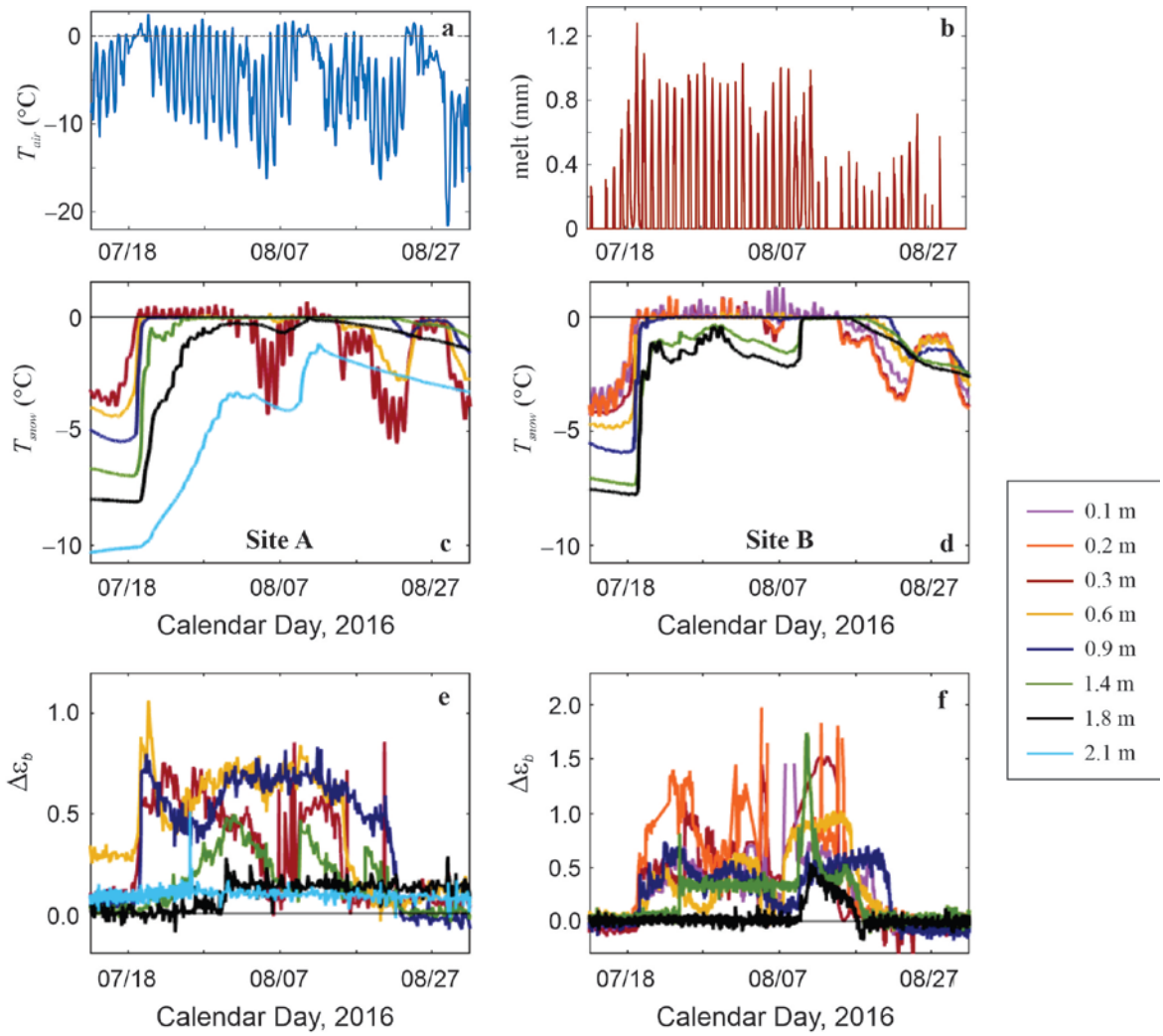

Figure 3. Same as Figure 2 but showing the main summer melt season from July 13 to September 1, 2016, and subsurface data in (c) to (f) are shown for the upper 2.1 m of the firn pits. Note the different scales in plots (e) and (f).

Overall, the evolution of subsurface temperatures and dielectric permittivities was similar at sites A and B, with evidence of thawing- and wetting-front propagation at the same times and to similar depths. Meltwater successfully penetrated several ice layers in the upper meter of firn at both sites. There were no ice layers in the winter snowpack, the upper ~0.9 m, but the underlying firn contained several discrete ice layers, some thin (1 mm to 2 cm), and others substantial. This included an 11-cm thick ice layer from 1.68 to 1.79 m depth at Site A and a 12-cm thick ice layer from 0.95 to 1.07 m depth at site B (Figure 1). In total over the upper 1.8 m, we measured 22 cm of ice in 11 discrete layers at site A and 19 cm of ice in 9 discrete layers at site B. Meltwater effectively penetrated through all of these ice layers, although not until temperatures reached the melting point at these depths.

4 Discussion

To our knowledge, these data represent the first continuous TDR measurements of meltwater infiltration in firn over a melt season. Combined with the thermistor records, the TDR data give a coherent account of the thermal evolution and meltwater infiltration at DYE-2 in summer 2016. The thawing front (0°C isotherm) and meltwater infiltration reached a depth of between 1.8 and 2.1 m. Below this, temperatures remained less than 0°C and dielectric permittivities did not rise above their background levels. This is in accord with observations from the upward-penetrating radar at site A, which also indicates penetration of the wetting front to about 2 m depth in summer 2016 (Heilig et al., 2018).

The data provide direct evidence of meltwater penetration through temperate ice layers in the Greenland percolation zone; ice layers did not act as impermeable barriers to meltwater infiltration. Rather, the depth of meltwater penetration at our sites was governed by the coupled hydrological and thermodynamic processes that determine the depth of the melting front (the 0°C isotherm). This in turn is a function of the net energy at the surface that is available to warm the snow and generate meltwater, the cold content, density, and structure (e.g., grain size) of the snow/firn (Colbeck, 1979; Colbeck and Anderson, 1982; Calonne et al., 2012), and the manner of meltwater infiltration, e.g., preferential flow processes (Humphrey et al., 2012; Hirashama et al., 2014; D'Amboise et al., 2017). The rate of melting is also important, through influences on near-surface saturation, refreezing capacity, and drainage processes.

The thawing/wetting front advanced to depth in step-wise fashion in our data. Four abrupt subsurface warming/wetting events were recorded over the summer, reaching progressively deeper into the snow and firn (Figures 2 and 3). These were seen simultaneously at the two sites and occurred during periods with positive air temperatures, but did not correspond to strong atmospheric warming events. Melt rates were high in these periods (Figures 2b and 3b), although not unusual. These events corresponded with increased or resumed surface melting following sustained cool (sub-zero) conditions. This indicates a potential role for restored cold content in the snow, which would increase refreezing capacity and latent heat release.

Subsurface warming occurs through a combination of latent heat release from meltwater refreezing, advective heat transfer associated with meltwater penetration into sub-zero snow, and thermal conduction, driven by heating of the surface layer in association with shortwave radiative fluxes and atmospheric warming. These mechanisms are clear in the thermistor data,

with gradual temperature shifts in response to atmospheric temperature fluctuations along with the abrupt subsurface warming events noted above. The sudden warming events are too rapid to be due to thermal conduction, so must be associated with meltwater advection and refreezing.

Modeled energy fluxes are described in detail in the Supplementary Material and illustrate the important role of latent heat flux in subsurface warming (Figure S4). Total summer latent heat release in the snow/firn is estimated to be 141 MJ m^{-2}, concentrated in the upper 0.3 m (Figure S4b). The model results give a good fit to the observational data and indicate that latent heat makes up 64.9% of the total summer (JJA) energy available to warm the subsurface snow and firn. Net energy at the surface during non-melt periods (i.e. sub-zero conditions) contributed an additional 76 MJ m^{-2} to warming the surface layer of the snowpack. This conductively warms the underlying snow and firn, accounting for 34.7% of the available subsurface energy. Positive net energy at the surface is particularly important in the early melt season (May and June), warming the snowpack prior to the onset of melt. After the onset of melt, meltwater infiltration drives deeper and more abrupt subsurface warming events, which are also captured in the model (Figure S4c). Meltwater advection made only a minor contribution to subsurface heat transport, estimated at 0.4% of the total energy available to warm the snow and firn.

Meltwater penetrated through multiple ice layers in the firn, permitting deeper meltwater infiltration and retention than would be possible if these layers acted as impermeable barriers. Two of the TDR sensors that experienced wetting were installed directly below thick, horizontally-continuous ice layers (sensors B6 and A5; see Figure 1c). While ice layers at our two sites were permeable, we can only speculate about the processes that permitted hydrological breakthrough. Fractures or discontinuities may have developed in the ice layers, or thawing to a temperate mixture of ice and water may have permitted water flux along interstitial grain boundaries and veins (e.g., Lliboutry, 1996). The effective permeability of ice layers and the relation to ice-layer thickness is an open question. There is evidence that thick ice layers in firn can be impermeable (Gascon et al., 2013; Ashmore et al., 2020), but meltwater infiltration through ice layers has also been observed or inferred (Humphrey et al., 2012; Machguth et al., 2016; Ashmore et al., 2020). Direct observations are needed to understand these processes and their efficacy with thicker ice layers, as found in the lower percolation zone of Greenland (Machguth et al., 2016; MacFerrin et al., 2019).

The similar evolution of the wetting front at our two sites, its progressive propagation to depth over the course of the melt season, the coherence with the upward-penetrating radar data near this site (Helig et al., 2018), and the ability to simulate the wetting front in a simple model of percolation flow (Figure S4) are all consistent with homogeneous infiltration of the wetting front. However, our measurements represent only two point locations, and the experimental design (vertically aligned sensors) does not permit conclusions concerning the mechanism(s) of meltwater infiltration. Preferential flow is thought to be the dominant process of meltwater infiltration in cold firn (e.g., Humphrey et al., 2012), and this may be what we recorded in summer 2016, if it proceeded in similar fashion at our two sites. Multiple instruments at each horizontal level would be needed to examine this.

Similarly, we cannot rule out meltwater penetration to depths greater than 2 m at other locations in the DYE-2 region in summer 2016. Spatial variability is a large challenge in understanding

and modeling firn hydrology and meltwater retention in Greenland. Our measurements nevertheless provide helpful insights to modelling efforts of meltwater infiltration into firn (*e.g.*, Wever et al., 2016; Steger et al., 2017), in particular the observation that ice layers can be permeable, permitting meltwater infiltration. Additional measurements like those reported here, especially during melt seasons of variable intensity, could help to track meltwater penetration into firn in the lower percolation zone and other sectors of Greenland.

Uncertainties

Sensor depths are reported as constant values in this manuscript, but actual depths changed over the course of the study, in association with fresh snowfall and surface ablation. Ultrasonic depth gauges were installed at each site to measure snow surface height (Figure S2d). All instruments at site A were deep enough to avoid melt-out. However, ablation from July 18 to August 9 was sufficient to expose the uppermost two sensors at site B (0.1 and 0.2 m), and inspection of the data is consistent with melt-out at these levels in the first week of August. A ~0.15 m snow event from August 10 to 12 buried the melted-out sensors and they give sensible signals again after this point, but data from August 5 to 12 are not reliable from these two levels.

There is a risk that water percolating in the disturbed area of the firn pits influences our sensors. although we see no evidence of this. The thermal and hydrological evolution are virtually identical at the two sites and are consistent with the upward-penetrating radar results of Helig et al. (2018), which measure the wetting front advance in undisturbed overlying firn. In addition, meltwater only penetrates to limited depths with each abrupt event; the pits were excavated to below the lower-most sensors, so free-flowing water in the disturbed areas would be expected to propagate deeper. Finally, the low rates of meltwater production and low-sloping environment at DYE-2 are more conducive to vertical infiltration than lateral flows. We are confident that the data reflect vertical meltwater infiltration from above, without influence from the adjacent pits, but this cannot be ruled out. Unfortunately, undisturbed control experiments are not feasible.

5 Conclusions

The thermistor, TDR, and AWS data provide a consistent and detailed account of the coupled thermodynamic and hydrological processes governing meltwater percolation and refreezing at DYE-2. This dataset presents an excellent opportunity to constrain the effective thermal and hydraulic conductivities of polar snow and firn, which will inform models of firn hydrology. Additional measurements are needed to test and confirm the inferred processes at other locations in Greenland's percolation zone.

Measurements from the two sites 400 m apart are exceptionally coherent, and indicate that meltwater at DYE-2 percolated to a depth of about 2 m in summer 2016. The wetting and melting fronts were coincident at the two sites, testifying to the coupled thermodynamic and hydrological controls on meltwater infiltration in firn. Meltwater penetrated through ice layers up to 12 cm thick. We are uncertain of the mechanical or thermodynamic processes that facilitate ice-layer permeability, but there is no evidence of meltwater infiltration through ice layers until temperatures reached 0°C. This requires sufficient latent heat release in the overlying firn and snow, which depends on the available pore space, cold content, and meltwater supply. Ice slabs

that are thick or close to the surface may be difficult to thaw, as heat transfer is reduced once firn is temperate or saturated. Models of this process can help to project whether meltwater is likely to infiltrate vertically or be redirected laterally, contributing to ice sheet runoff.

Acknowledgements

We thank Baptiste Vandecrux, Darren Hill, Achim Heilig, Liam Colgan, Bastian Gerling, and Leander Gambal for support with the field work. The U.S. National Science Foundation, Air National Guard, and CH2MHill Polar Field Services provided essential logistical support for this field work. Research costs of SS and SJM were supported by the Natural Sciences and Engineering Research Council (NSERC) of Canada, and funding for MM and the FirnCover project was from NASA Award NNX15AC62G. Data from this study are archived in the University of Calgary data repository, https://doi.org/10.5683/SP2/2QY39K. The authors declare no conflict of interest with the methods or results of this study.

References

Ashmore D. W, Mair D. W. F., and Burgess, D. O. (2020). Meltwater percolation, impermeable layer formation and runoff buffering on Devon Ice Cap, Canada. *Journal of Glaciology*, *66* (255), 61-73, https://doi.org/ 10.1017/jog.2019.80

Bamber, J. L., Westaway, R. M., Marzeion, B., & Wouters, B. (2018). The land ice contribution to sea level during the satellite era. *Environmental Research Letters*, *13* (6), 1–21.

Brock, B. W., Willis, I. C., & Sharp, M. J. (2006). Measurement and parameterisation of aerodynamic roughness length variations at Haut Glacier D'Arolla, Switzerland. *Journal of Glaciology*, *52* (177), 281–297

Calonne, N., Geindreau, C., Flin, F., Morin, S., Lesaffre, B., Rolland du Roscoat, S., & Charrier, P. (2012). 3-D image-based numerical computations of snow permeability: links to specific surface area, density, and microstructural anisotropy. *The Cryosphere*, *6*, 939–951, https://doi.org/10.5194/tc-6-939-2012.

Colbeck, S. C. (1979). Water flow through heterogeneous snow. *Cold Regions Science and Technol*ogy, *1*, 37–45, https://doi.org/10.1016/0165- 232X(79)90017-X.

Colbeck, S. C., & Anderson, E. A. (1982). The permeability of a melting snow cover. *Water Resources Research*, *18* (4), 904-908, https://doi.org/10.1029/WR018i004p00904.

Cuffey, K. M., & Paterson, W. S. B. (2010). *The Physics of Glaciers*, 4th Ed.

D'Amboise, C. J. L., Müller, K., Oxarango, L., Morin, S., and Schuler, T. V. (2017). Implementation of a physically based water percolation routine in the Crocus/SURFEX (V7.3) snowpack model. *Geoscience Model Development*, *10*, 3547–3566, https://doi.org/10.5194/gmd-10-3547-2017.

Denoth, A. (1994). An electronic device for long-term snow wetness recording. *Annals of Glaciology*, *19* (1), 104-106, https://doi.org/10.3189/S0260305500011058.

Ebrahimi, S., & Marshall, S. J. (2016). Surface energy balance sensitivity to meteorological variability on Haig Glacier, Canadian Rocky Mountains, *The Cryosphere*, *10*, 2799–2819, https://doi.org/10.5194/tc-10-2799-2016.

Forster, R. R., Box, J. E., van den Broeke, M. R., Miège, C., Burgess, E. W., Van Angelen, J. H., et al. (2014). Extensive liquid meltwater storage in firn within the Greenland ice sheet. *Nature Geoscience*, *7* (2), 95-98, https://doi.org/10.1038/ngeo2043.

Gascon, G., Sharp, M., Burgess, D., Bezeau, P., and Bush, A. B. G. (2013). Changes in accumulation-area firn stratigraphy and meltwater flow during a period of climate warming: Devon Ice Cap, Nunavut, Canada, *Journal of Geophysical Research, Earth Surfaces, 118*, 2380–2391, doi:10.1002/2013JF002838.

Harper, J., Humphrey, N., Pfeffer, W. T., Brown, J., & Fettweis, X. (2012). Greenland ice-sheet contribution to sea-level rise buffered by meltwater storage in firn. *Nature*, *491*, 240–243, doi: 10.1038/nature11566.

Heilig, A., Eisen, O., MacFerrin, M., Tedesco, M., & Fettweis, X. (2018). Seasonal monitoring of melt and accumulation within the deep percolation zone of the Greenland Ice Sheet and comparison with simulations of regional climate modeling. *Cryosphere*, *12*, 1851-1866. Doi: 10.5194/tc-12-1851-2018

Hirashima, H., Yamaguchi, S., & Katsushima, T. (2014). A multidimensional water transport model to reproduce preferential flow in the snowpack, *Cold Regions Science and Technology*, *108*, 80–90, https://doi.org/10.1016/j.coldregions.2014.09.004.

Humphrey, N. F., Harper, J. T., & Pfeffer, W. T. (2012). Thermal tracking of meltwater retention in Greenland's accumulation area. *Journal of Geophysical Research, 117*, F01010. https://doi.org/10.1029/2011JF002083.

Koenig, L. S., Miège, C., Forster, R. R., & Brucker, L. (2014). Initial in situ measurements of perennial meltwater storage in the Greenland firn aquifer. *Geophysical Research Letters, 41* (1), 81-85, https://doi.org/10.1002/2013GL058083.

Lliboutry, L. (1996). Temperate ice permeability, stability of water veins, and percolation of internal meltwater. *Journal of Glaciology*, *42* (141), 210-211.

MacFerrin, M., Machguth, H., van As, D., Charalampidis, C., Stevens, C. M., A. Heilig, A., et al. (2019). Rapid expansion of Greenland's low-permeability ice slabs. *Nature*, 573, 403-407, doi:10.1038/s41586-019-1550-3.

Marks, D., & Dozier, J. (1992). Climate and energy exchange at the snow surface in the Alpine region of the Sierra Nevada: 2. Snow cover energy balance. *Water Resources Research*, *28*, 3043–3054, https://doi.org/10.1029/92WR01483.

Mouginot, J., Rignot, E., Bjørk, A. A., van den Broeke, M., Millan, R., Morlighem, M., et al. (2019). Forty-six years of Greenland Ice Sheet mass balance from 1972 to 2018. *Proceedings of the U.S. National Academy of Sciences*, *116* (19), 9239-9244, https://doi.org/10.1073/pnas.1904242116.

Noël, B., van de Berg, W. J., Lhermitte, S., Wouters, B., Machguth, H., Howat, I., et al. (2017). A tipping point in refreezing accelerates mass loss of Greenland's glaciers and ice caps. *Nature Communications*, *8* (1), 1-8, doi:10.1038/ncomms14730.

Pfeffer, W. T., M. F. Meier, & Illangasekare, T. H. (1991). Retention of Greenland runoff by refreezing: Implications for projected future sea level change, *Journal of Geophysical Research*, *96* (C12), 22117–22124, doi:10.1029/91JC02502.

Pfeffer, W. T., & Humphrey, N. F. (1998). Formation of ice layers by infiltration and refreezing of meltwater. *Annals of Glaciology*, *26*, 83-91, https://doi.org/10.3189/*1998AoG26*-1-*83-91*.

Rennermalm, A. K., Moustafa, S. E., Mioduszewski, J., Chu, V. W., Forster, R. R., Hagedorn, B., et al. (2013). Understanding Greenland ice sheet hydrology using an integrated multi-

scale approach. *Environmental Research Letters*, *8* (1), 015017, doi: 10.1088/1748-9326/8/1/015017.

Samimi, S., & Marshall, S. J. (2017). Diurnal cycles of meltwater percolation, refreezing, and drainage in the supraglacial snowpack of Haig glacier, Canadian Rocky Mountains. *Frontiers in Earth Science*, *5*, 6, https://doi.org/10.3389/feart.2017.00006.

Schneebeli, M., Coléou, C., Touvier, F. & Lesaffre, B. (1998). Measurement of density and wetness in snow using time-domain reflectometry. *Annals of Glaciol*ogy, *26*, 69-72, https://doi.org/10.3189/*1998AoG26*-1-*69-72*.

Steger, C. R., Reijmer, C. H., van den Broeke, M. R., Wever, N., Forster, R. R., Koenig, L. S., et al. (2017). Firn meltwater retention on the Greenland Ice Sheet: a model comparison. *Frontiers in Earth Science*, *5* (3), https://doi.org/10.3389/feart.2017.00003.

Stein, J., Laberge, G., & Lévesque, D. (1997). Monitoring the dry density and the liquid water content of snow using time domain reflectometry (TDR). *Cold Regions Science and Technology*, *25* (2), 123-136, doi:10.1016/S0165-232X(96)00022-5.

Techel, F., & Pielmeier, C. (2011). Point observations of liquid water content in wet snow – investigating methodical, spatial and temporal aspects. *The Cryosphere*, *5*, 405-418, doi:10.5194/tc-5-405-2011.

van As, D., Box, J. E., & Fausto, R. S. (2016). Challenges of quantifying meltwater retention in snow and firn: an expert elicitation. *Frontiers in Earth Science*, *4* (101), https://doi.org/10.3389/feart.2016.00101.

van den Broeke, M., Bamber, J., Ettema, J., Rignot, E., Schrama, E., van de Berg, W. J., et al. (2009). Partitioning recent Greenland mass loss. *Science*, *326* (5955), 984-986, doi: 10.1126/science.1178176.

Vandecrux, B., MacFerrin, M., Machguth, H., Colgan, W. T., van As, D., Heilig, A., et al. (2019). Firn data compilation reveals widespread decrease of firn air content in western Greenland. *The Cryosphere*, 13, 845–859, https://doi.org/10.5194/tc-13-845-2019.

Verjans, V., Leeson, A. A., Stevens, C. M., MacFerrin, M., Noël, B., & van den Broeke, M. R. (2019). Development of physically-based liquid water schemes for Greenland firn-densification models. *The Cryosphere*, 13, 1819-1842, https://doi.org/10.5194/tc-13-1819-2019.

Vernon, C. L., Bamber, J. L., Box, J. E., van den Broeke, M. R., Fettweis, X., Hanna, E., & Huybrechts, P. (2013). Surface mass balance model intercomparison for the Greenland ice sheet. *The Cryosphere*, *7*, 599–614, https://doi.org/10.5194/tc-7-599-2013.

Wever, N., Würzer, S., Fierz, C., & Lehning, M. (2016). Simulating ice layer formation under the presence of preferential flow in layered snowpacks. *The Cryosphere*, *10*, 2731–2744, https://doi.org/10.5194/tc-10-2731-2016.

Geophysical Research Letters

Supporting Information for

Meltwater Penetration Through Temperate Ice Layers in the Percolation Zone at DYE-2, Greenland Ice Sheet

Samimi, S.[1], S.J. Marshall[1,2] and M. MacFerrin[3]

[1] Department of Geography, University of Calgary, Calgary, Alberta, Canada
[2] Environment and Climate Change Canada, Gatineau, Quebec, Canada
[3] Cooperative Institute for Research in Environmental Sciences, University of Colorado, Boulder, CO, USA

Contents of this file

Additional Supporting Information (Files uploaded separately)

Introduction

Details of the firn thermistor, time-domain reflectometry (TDR), and automatic weather station (AWS) data from summer 2016 are included here. Figure S1 shows the location of the study, at DYE-2 in southwestern Greenland, along with our two firn pits, referred to as Sites A and B. Figure S2 plots the measured air temperature and snow surface height/snow depth data, along with the calculated surface energy balance and melt at the AWS site. Figure S3 illustrates the full evolution of the air, snow, and firn temperatures and the dielectric permittivities at Site A through summer 2016. We also provide details of the surface energy balance and subsurface thermal/hydrological model, and Figure S4 presents model results for the subsurface temperature evolution and the energy fluxes associated with refreezing and meltwater advection.

Data from this study are being archived at the University of Calgary data repository, and are also provided with the Supporting Information as Excel files. This is directly from the datalogger download, without processing, but missing or off-scale data values (-99999) have been replaced by either NaN or an empty cell.

Text S1

Figure S1 shows the location of the study in southwestern Greenland, including our two firn pits (sites A and B). Co-ordinates of each firn pit are included in Table S1, along with details of the initial snow temperature, density, dielectric permittivity, and sensor installation depths.

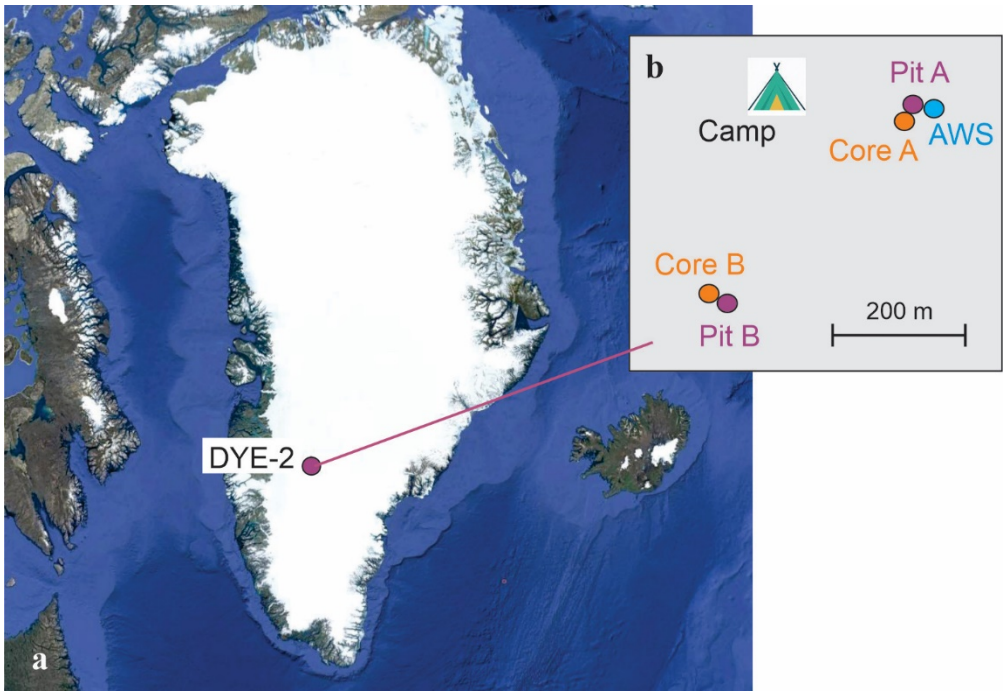

Figure S1. Study site at DYE-2, southwestern Greenland. AWS refers to the automatic weather station. Firn pits A and B were 402 m apart. Image (a) courtesy of Google Earth.

An automatic weather station (AWS) was set up on a tripod adjacent to firn pit A. The AWS was configured to measure air temperature, relative humidity, air pressure, incoming and outgoing shortwave and longwave radiation (Kipp and Zonen CNR1 radiometer), wind speed and direction, and snow surface height, based on an SR50A ultrasonic depth sounder. The SR50A sensor was installed separately on a pole drilled into the firn, in order to maintain a fixed height while the snow surface changed. Air

temperature, relative humidity, and snow surface height were also measured at firn pit B. All sensors were wired to CR1000 Campbell Scientific dataloggers at each site and were programmed to record 30-minute averages of 10-second measurements.

The AWS was installed on April 28, 2016 and was left in place until spring 2017, when we returned to the site to collect data and take the station down. Data were recorded continuously from the time of installation until November 2016, at which point the battery weakened due to insufficient solar charging. There are no data gaps in the AWS record from April 28 through October 28, 2016. This study focuses on the meteorological conditions and surface energy balance from May to September, 2016, covering the complete 2016 melt season.

	Site A (installed 16/05/11) 66.47775°N, 46.28510°W				Site B (installed 16/05/08) 66.47505°N, 46.29115°W			
Level	d (m)	T_{s0} (°C)	ε_{b0}	ρ_0 (kg m^{-3})	d (m)	T_{s0} (°C)	ε_{b0}	ρ_0 (kg m^{-3})
1	0.3	–7.3	2.37	380	0.1	–3.7	2.31	280
2	0.6	–10.1	1.88	380	0.2	–4.2	2.49	310
3	0.9	–12.7	2.21	230	0.4	–6.6	2.09	280
4	1.4	–14.5	2.32	510	0.6	–9.2	2.06	320
5	1.8	–15.1	2.37	410	0.9	–11.9	2.47	640
6	2.1	–15.6	2.44	460	1.2	–13.1	2.54	620
7	2.8	–15.7	2.14	360	1.5	–14.4	2.65	560
8	3.7	–15.8	2.67	520	1.6	–14.9	2.36	480

Table S1. Installation depths (d) and initial snow/firn temperature (T_0), bulk dielectric permittivity (ε_{b0}), and density (ρ_0) at each measurement level for sites A and B.

Surface Energy Balance Model

The surface energy balance was calculated following the model of Ebrahimi and Marshall (2016), including a subsurface model for heat conduction in the upper 10 m of firn and snow, the approximate depth of penetration of the annual temperature wave (Cuffey and Paterson, 2010). Net energy at the ice sheet surface is a function of the energy fluxes at the surface-atmosphere interface,

$$Q_N = Q_S^{\downarrow}(1-\alpha) + Q_L^{\downarrow} - Q_L^{\uparrow} + Q_H + Q_E + Q_C\,, \quad (1)$$

where $Q_S^{\downarrow}$ is the incoming shortwave radiation, α is the surface albedo, $Q_L^{\downarrow}$ and $Q_L^{\uparrow}$ are the incoming and outgoing longwave radiation, Q_H and Q_E are the sensible and latent heat fluxes, and Qc is the upward-directed conductive heat flux from the snow/firn to the

surface. All energy fluxes have units W m^{-2} and are defined to be positive when they are sources of energy to the surface. Energy fluxes associated with precipitation are assumed to be negligible.

When the surface temperature is below 0°C, net energy Q_N goes to heating or cooling the surface layer of the snow/firn, a 0.1-m layer within the subsurface model. If the surface is at 0°C and $Q_N > 0$, net energy goes to melting, following

$$\dot{m} = Q_N/(\rho_w L_f), \quad (2)$$

where $\dot{m}$ is the melt rate (m s^{-1}), and L_f is the latent heat of fusion. If net energy is negative, any liquid water that is present will refreeze and then the surface layer will cool.

To calculate net energy in Eq. (1), radiation fluxes were directly measured and the turbulent fluxes were modelled using a bulk aerodynamic approach (e.g., Andreas, 2002),

$$Q_H = \rho_a c_p k^2 v \left[\frac{T_a(z)-T_s}{\ln(z/z_0)\ln(z/z_{0H})}\right], \quad (3)$$

and

$$Q_E = \rho_a L_v k^2 v \left[\frac{q_a(z)-q_s}{\ln(z/z_0)\ln(z/z_{0E})}\right]. \quad (4)$$

Here T_a, q_a and v are the air temperature, specific humidity, and wind speed measured at the AWS, T_s and q_s are the temperature and specific humidity at the snow surface, ρ_a is the air density, c_p is the specific heat capacity of air, L_v is the latent heat of evaporation, and k = 0.4 is von Karman's constant. Parameters z_0, z_{0H}, and z_{0E} refer to the roughness length scales for turbulent exchange of momentum, heat, and moisture. We adopt fixed roughness values based on typical values for snow-covered glaciers (Brock et al., 2006), z_0 = 1 mm and $z_{0H} = z_{0E} = z_0/100$. We estimate the surface skin temperature T_s from an inversion of Stefan-Boltzmann's equation, using measurements of outgoing longwave radiation. The surface humidity q_s can then be calculated from the saturation specific humidity over snow at temperature T_s.

Conductive heat flux to the ice sheet surface, Q_C, is calculated from the vertical heat conduction in the upper three layers of the subsurface model (described in more detail below), based on a three-point forward finite difference:

$$Q_C = -\frac{k_t}{2\Delta z}(3T_1 - 4T_2 + T_3). \quad (5)$$

for thermal conductivity k_t and layer thickness Δz. The surface energy balance is calculated every 30 minutes based on the AWS data, Eqs. (3)-(5), and the subsurface temperature model, giving an estimate of 30-minute melt amounts over summer 2016.

Subsurface Temperature Model

The subsurface model includes a simple one-dimensional treatment of the coupled thermodynamic and hydrological evolution in the upper 10 m of snow and firn, including a simple treatment of meltwater percolation and refreezing (Samimi and Marshall, 2017). The model has 33 layers, denoted z_k, for $k \in [1,33]$, with layer thickness Δz_k. Resolution is concentrated near the surface; layers are 0.1-m thick from the surface to a depth of 0.6 m, 0.2-m thick from 0.6 to 2 m, and 0.4-m thick from 2 to 10 m.

The thermal evolution in each subsurface layer is a function of vertical heat conduction, latent heat release from meltwater refreezing, and heat advection by meltwater:

$$\rho_s c_s \frac{\partial T}{\partial t} = \frac{\partial}{\partial z}\left(-k_t \frac{\partial T}{\partial z}\right) + \varphi_t + \rho_w c_w q_w \frac{\partial T_w}{\partial z}, \quad (6)$$

where ρ_s and c_s, are the density and specific heat capacity of the subsurface snow or firn, ρ_w and c_w are the density and specific heat capacity of water, and q_w is the vertical rate of meltwater percolation, with units m s^{-1}. The second term on the right-hand-side, φ_t, represents latent heat release from refreezing, with units W m^{-3}, calculated from

$$\varphi_t = \frac{\rho_w L_f \dot{r}}{\Delta z}, \quad (7)$$

where $\dot{r}$ is the refreezing rate (m s^{-1}) and this heat is spread across the layer thickness. The final term in Eq. (6) describes heat advection from meltwater flow, where the temperature derivative $\partial T_w/\partial z$ is with reference to the meltwater, which is assumed to have a temperature of 0°C. Meltwater can percolate downward from layer k to layer k+1, which has temperature $T_{k+1} \leq 0$°C. If the layer is temperate (T_{k+1} = 0°C), there is no heat advection. If it is below 0°C, the firn temperature is adopted in $\partial T_w/\partial z$ and heat advection is calculated from $-\rho_w c_w q_w T_{k+1}/\Delta z$, for $\Delta z = z_k - z_{k+1}$. For the upper layer, the melt rate, $\dot{m}$, is taken as the percolation velocity and Δz is equal to the thickness of the upper layer.

Refreezing occurs when water percolates into a sub-zero layer, accompanied by latent heat release calculated from Eq. (6). Once a layer is temperate, liquid water can be retained within the pore space or it can percolate deeper into the snow or firn. We adopt a simple model for the water flux, $q_w = -k_h \nabla \emptyset$, for hydraulic conductivity k_h and hydraulic potential $\emptyset$ (in m). If conductive energy loss occurs in a subsurface layer where liquid water is present, refreezing takes place before the firn will cool, following Eq. (5). Temperatures cannot drop below 0°C until all of the liquid water is refrozen.

The subsurface model was initiated with the observed snow/firn thermistor temperatures and snow densities at the time of installation for the upper 3.5 m of the snow and firn. Below this, the density and temperature were extrapolated to 10 m depth for the initial conditions. The subsurface model is forced by the net energy and surface melt in the upper layer, calculated from Eqs. (1) and (2).

Surface Energy Balance Results

Figure S2 plots the surface energy balance and modelled melt through summer 2016, along with air temperature and snow depth data fromt the AWS located adjacent to firn pit A. Air temperatures first reached 0°C in mid-May but then cooled again until the main melt season from the second week of June through to late August (Figure S2a).

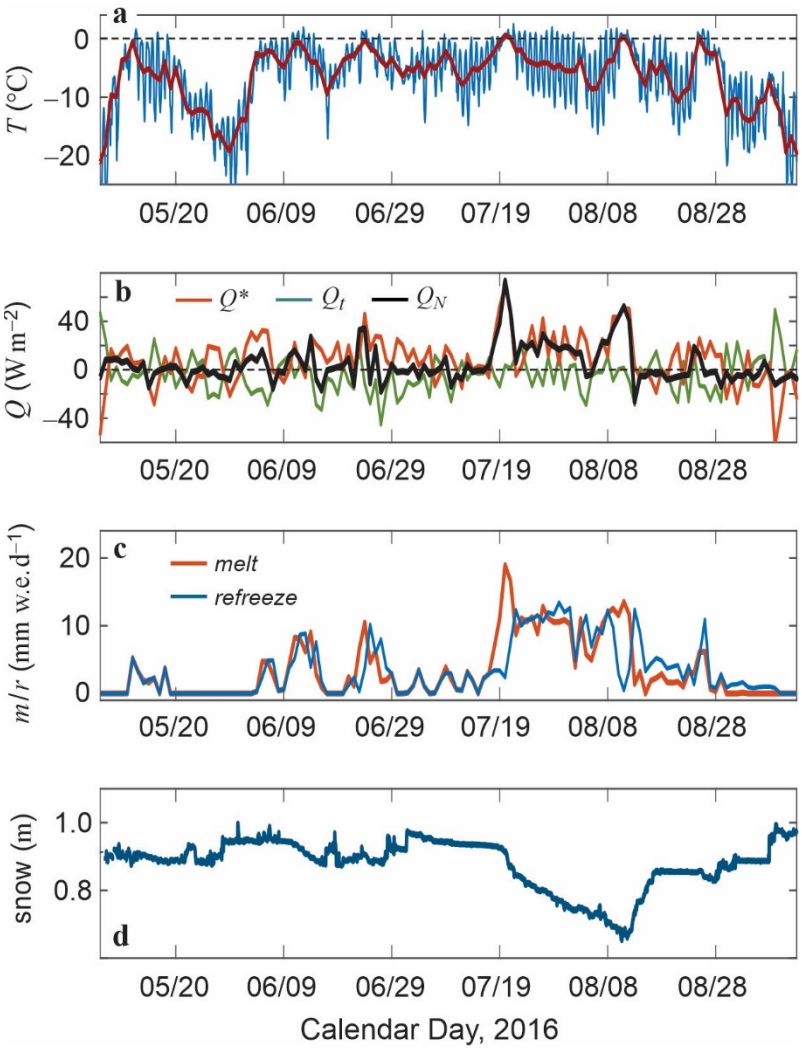

Figure S2. Automatic weather station (AWS) and surface energy balance data from DYE2, May 5 to Sept 11, 2016. (a) Mean daily (red) and 30-minute (blue) air temperature, °C. (b) Mean daily net radiation (Q*), turbulent (Q_t), and net energy (Q_N) fluxes. (c) Modelled daily melt and refreezing, m w.e. (d) Measured snow surface height (m). The initial snow depth was 0.9 m at the time of AWS installation.

Figure S2 plots air temperature, surface energy balance, and modeled melt at the AWS site from May through September, 2016, with results of the surface energy balance and melt model discussed in detail in the Supporting Information. Frequent daily maximum air temperatures above 0°C began in the first week of June and continued through late August, with a return to persistent sub-zero air temperatures after August 26. The main summer melt period was from July 18 to August 9 (Figure S2c). We estimate a total summer melt of 0.51 m w.e., with 0.22 m w.e. of melt from the seasonal snowpack. Meltwater retained near the surface melts and refreezes multiple times in association with diurnal freeze-thaw cycles, such that meltwater is commonly 'recycled', i.e. net energy is used to melt the same snow (and resulting near-surface ice layers and pore water) more than once. Ultrasonic depth gauges installed adjacent to each firn pit recorded a total surface drawdown of ~0.5 m over the summer (Figure S2d), largely offset by several periods of snow accumulation. Snow surface height decreased from its initial value of 0.9 m to a minimum value of 0.66 m on August 9 (Figure S2d), associated with the main period of melting. These data are consistent with the modeled melt, but we note that snow surface lowering also occurs from snow/firn compaction, sublimation, and wind scour. It is difficult to separate these processes in the observational data, so the snow surface height record is not a direct measure of surface melting.

Figure S3 plots the evolution of subsurface snow/firn temperature and dielectric permittivity over the summer melt season at Site A. Liquid water content was consistently detected in association with temperate (0°C) conditions through the melt season, providing a coherent picture of the co-development of thermal and hydrological conditions in the firn. At the time of sensor installation, near-surface firn was in the process of warming from the winter. The snow at 0.3 m depth first warmed to the melting point and showed evidence of liquid water on June 23, roughly two weeks after the initial positive air temperatures. Diurnal cycles of surface melting continued regularly into mid-August (Figure S1), accompanied by firn warming and meltwater infiltration to a depth of between 1.8 and 2.1 m. Sensors at and below 2.1 m depth remained frozen and dry.

Figure S2b plots mean daily energy fluxes at the glacier surface over the summer melt season, including the net radiation, $Q^* = Q_S^{\downarrow}(1-\alpha) + Q_L^{\downarrow} - Q_L^{\uparrow}$, the combined turbulent and conductive fluxes, $Q_t = Q_H + Q_E + Q_C$, and the net energy, Q_N. Mean daily net radiation is near 0 for much of the summer, but is strongly positive on during two periods of heavy cloud cover on July 18-19 and August 9-11, which mark the beginning and end of the main summer melt period. During this period and overall for the summer, net energy is most strongly correlated with net radiation (r = 0.68), compared with a linear correlation coefficient of r = 0.48 for the turbulent fluxes. The mean summer (JJA) net energy was 5.4 W m^{-2}.

Total modelled melt from May through September was calculated to be 0.51 m w.e.

(Figure S2c). Of this, 60% (0.30 m w.e.) melted during the main summer ablation period from July 17 to August 11. All of the melt refroze within the snow and firn, with much of the refreezing occurring in the near-surface (upper 0.1 m). Near-surface ice layers went through successive melt-freeze cycles, such that the actual summer ablation was much less than the total melt. That is, melt energy was used to melt the same snow/ice more than once. The total modelled summer snow melt was 0.22 m w.e.; the remaining 0.29 m w.e. of melting consisted of refrozen ice layers, i.e. recycled meltwater.

This result is consistent with the ultrasonic depth gauge record of snow surface height change, plotted in Figure S2d. These data show several periods of summer snow accumulation, through either snowfall or wind loading, balanced against surface height reductions due to a combination of ablation and densification. The surface height is plotted with reference to the initial (late April) snow thickness of 0.9 m. Cumulative surface height reductions through the summer totaled ~0.5 m, with periods of surface drawdown strongly aligned with the active melt periods. Based on measured snow densities, the 0.22 m w.e. of modelled melt should give a surface drawdown of ~0.54 m, so most of the SR50 signal can be attributed to melting. Compaction immediately following fresh-snow events is visible in the SR50 signal, but densification of deeper snow and firn may have caused sinking of the SR50 pole, masking the surface height signal due to snow/firn compaction.

Thermistor and TDR Data from Firn Pit A

Figure S3 plots the evolution of the summer melt season at firn pit A. Air temperatures first reached 0°C in mid-May but then cooled again until the main melt season, which extended from the second week of June through to mid-August (Figure S3a). Snow surface temperature in Figure S3a is calculated from an inversion of the measured outgoing longwave radiation: $T_s = (Q_L^{\uparrow}/\sigma E_s)^{1/4}$, assuming a surface emissivity E_s of 0.98 (Marks and Dozier, 1992).

At the time of sensor installation, the snow and firn were still frozen and dry, Subsurface temperatures were between −7 and −16°C, decreasing with depth, and initial dielectric permittivity, ε_{b0}, ranged from 1.9 and 2.7 (Table S1). These are all dry-snow values, with some of the difference due to local snow and firn density (Schneebeli et al., 1998); because ice has a greater dielectric permittivity than air, dense snow and firn have higher values of ε_{b0}. The correlation coefficient is 0.55 in our data; hence, other factors such as TDR coupling, grain size and morphology, or potential snow compaction on insertion of the TDR probes also appear to influence ε_{b0}.

Figures S3b and S3c plot subsurface temperatures and dielectric permittivities in the upper 3.7 m of snow and firn at site A through summer 2016. To simplify the plot and focus on the meltwater signal at different depths, dielectric permittivities are plotted as anomalies relative to the initial value for each sensor, $\Delta\varepsilon_b(t) = \varepsilon_b(t) - \varepsilon_{b0}$. Changes in ε_b

over the summer are associated with either densification (a gradual increase in ε_b) or wetting/drying of the snow, which produces abrupt increases/decreases in ε_b.

Data in Figure S3 were quality-controlled to reject unphysical values and gap-fill any missing data through linear interpolation. The thermistor and automatic weather station data were complete, with no errant values, but TDR data gaps were frequent, giving rejection rates of 32 to 81% for the individual sensors at site A. TDR data were also much more complete at site B: from 74 to 99% for individual sensors, with an average of 94%. We are unsure why the TDR records from this site have less data gaps than at Site A. It is possible that electromagnetic signals at Site A were impacted by the adjacent AWS (which reported to the same datalogger) or the upwards-looking snow radar that was installed ~5 m from the TDR installation. The TDR sensors give a noisy signal compared to the thermistors, but the combined records provide a reliable account of the coupled thermal and hydrological evolution in the near-surface firn over summer 2016.

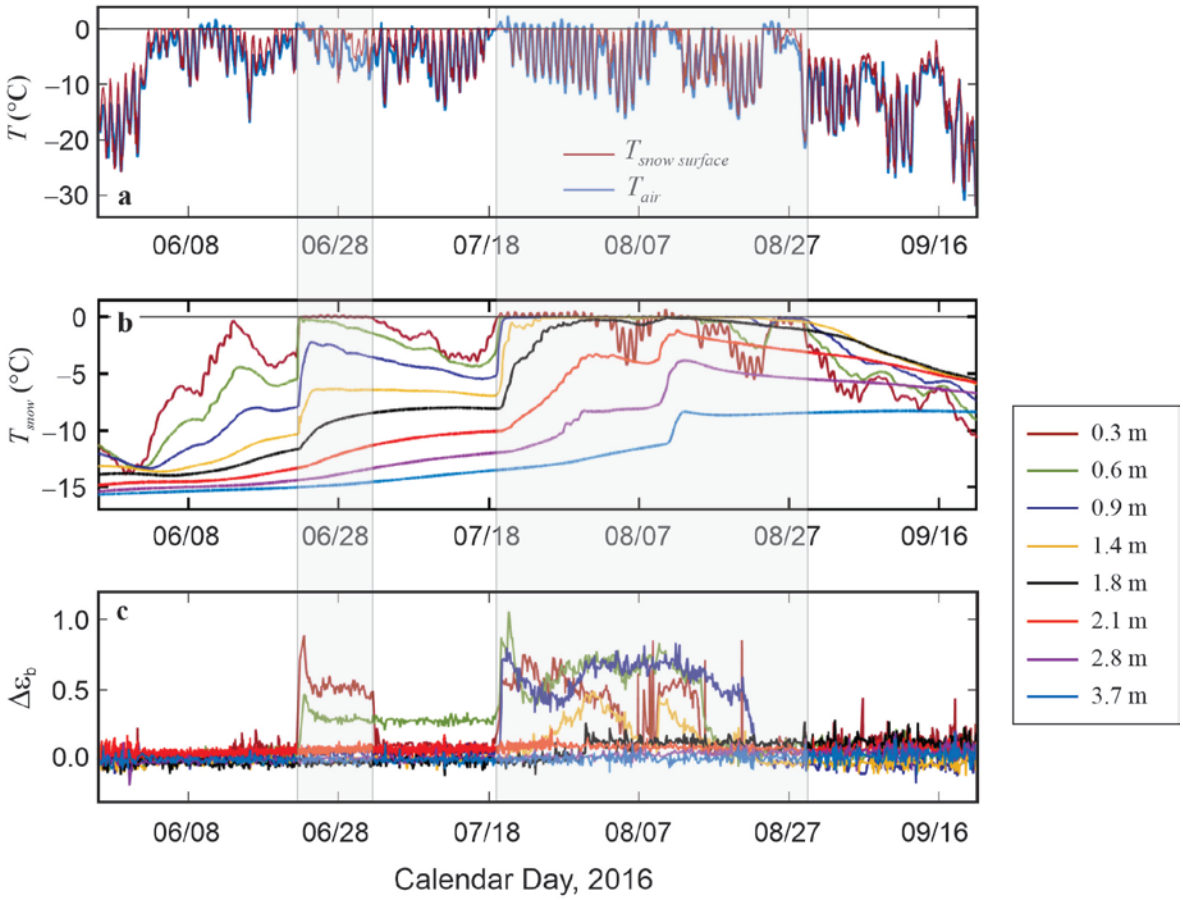

Figure S3. Measured (a) air and snow surface temperatures, (b) snow temperatures, and (c) dielectric permittivity anomalies in firn pit A, May 27 to Sept 21, 2016. Shaded areas indicate periods with temperate snowpack conditions, based on the thermistor records.

Modelled Subsurface Energy Fluxes

The firn model, driven by the AWS data, facilitates a detailed examination of the subsurface energy fluxes and coupled hydrological and thermodynamic processes. Model details and sensitivities will be discussed in a followup manuscript, but Figure S4 plots the results of a simulation that gives a good fit to the observed firn temperature and TDR data in summer 2016. Figure S4c shows the simulated temperature evolution in the upper 4 m of the snow and firn, capturing the observed rapid warming events and the penetration of the melting/wetting front to approximately 2 m depth in August.

The warming events are associated with meltwater infiltration and latent heat release. Where meltwater enters a sub-zero snow layer with temperature T_k, there is an associated heat advection, calculated from:

$$E_{adv} = -\rho_w c_w q_w T_k \,, \tag{8}$$

with units J m^{-2}. There can similarly be an advection of energy out of the layer if meltwater is percolating to a greater depth. The latent heat release from refreezing is calculated from:

$$E_{ref} = \rho_w L_f \dot{r} \,, \tag{8}$$

also with units J m^{-2}. Integrated values of these two energy fluxes are plotted in Figures S4a and S4b for the summer melt season. Figure S4a shows total daily energy released by each process, integrated over the depth of the firn, and Figure S4b plots the energy release as a function of depth, integrated over the melt season. Latent heat release dominates the subsurface energy transport associated with meltwater infiltration, totalling 141 MJ m^{-2} over the summer (JJA) compared with 0.9 MJ m^{-2} for the heat transport from meltwater advection.

Also shown in Figure S4a are the total daily surface energy fluxes associated with melting and warming the snowpack. These are calculated from the amount of positive net energy that is directed to each. The total summer (JJA) energy flux directed to melt equals 141 MJ m^{-2}, identical to the latent heat release from refreezing as 100% of the meltwater refreezes locally. The total summer (JJA) net energy directed to warming of the surface layer equals 76 MJ m^{-2}; much of this energy is conducted downwards into the snow and firn. Latent heat release is the primary source of energy for subsurface warming (64.9%), but net energy at the surface that is directed to warming of the snow and firn is also significant (34.7%). Advective heat transfer by meltwater percolation accounted for the remaining 0.4%. In the months of May and September, warming energy exceeds melt energy (62 vs. 6 MJ m^{-2}), but there is little melt in these months; firn warming is concentrated in the main summer melt season in the months of July and August (Figure S4c), when meltwater infiltration plays a critical role in transporting latent

energy to depth.. The net energy directed to warming in May is, however, important to priming the snow and firn for the melt season.

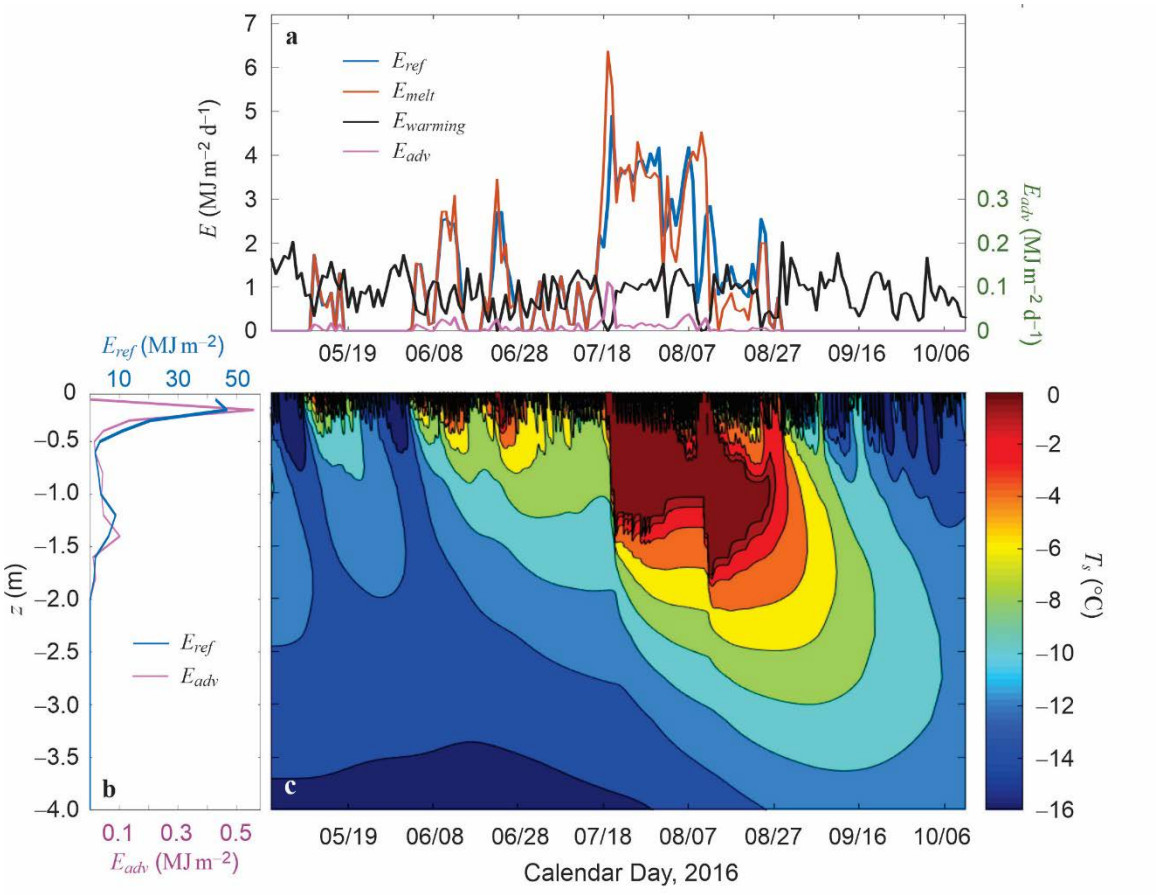

Figure S4. Modelled surface and subsurface energy fluxes and temperatures in the upper 4 m of snow and firn from May 1 to October 10, 2016. (a) Daily surface energy (MJ m^{-2} d^{-1}) directed to melting and warming the snow/firn, along with the subsurface energy release due to refreezing (*ref*) and meltwater advection (*adv*). (b) Depth profile of subsurface energy release due to latent heat of refreezing and meltwater advection, integrated over the full summer melt season. Note the different scales. (c) Subsurface temperature evolution in the upper 4 m, with the 0°C isotherm (wetting front) reaching a maximum depth of 1.9 m in the second week of August.

Supplementary References

Brock, B.W., Willis I. C., & Sharp, M. J. (2006). Measurement and parameterisation of aerodynamic roughness length variations at Haut Glacier D'Arolla, Switzerland. *Journal of Glaciology*, *52* (177), 281–297

Cuffey, K. M., & Paterson, W. S. B. (2010). *The Physics of Glaciers*, 4th Ed.

Ebrahimi, S., & Marshall, S. J. (2016). Surface energy balance sensitivity to meteorological variability on Haig Glacier, Canadian Rocky Mountains, *The Cryosphere*, *10*, 2799–2819, https://doi.org/10.5194/tc-10-2799-2016.

Marks, D., & Dozier, J. (1992). Climate and energy exchange at the snow surface in the Alpine region of the Sierra Nevada: 2. Snow cover energy balance. *Water Resources Research*, *28*, 3043–3054, https://doi.org/10.1029/92WR01483.

Samimi, S., & Marshall, S. J. (2017). Diurnal cycles of meltwater percolation, refreezing, and drainage in the supraglacial snowpack of Haig glacier, Canadian Rocky Mountains. *Frontiers in Earth Science*, *5*, 6, https://doi.org/10.3389/feart.2017.00006.

Schneebeli, M., Coléou, C., Touvier, F. & Lesaffre, B. (1998). Measurement of density and wetness in snow using time-domain reflectometry. *Annals of Glaciol*ogy, *26*, 69-72, https://doi.org/10.3189/*1998AoG26*-1-69-72.

Data Set S1. The dataset for this study is being archived at the University of Calgary data repository, and is also available on request from the authors. AWS, TDR, and thermistor data were written to a Campbell Scientific CR1000 datalogger and the raw (ascii) output from the datalogger is imported to an Excel spreadsheet. Data have been quality-controlled through the elimination of any non-physical values (e.g., -99999); these are replaced with NaN or blanks in the dataset. In the publication figures, linear interpolation was used in MATLAB to gap-fill missing TDR data. The thermistor and AWS data were complete. Ultrasonic depth gauge (SR50A) data were filtered to remove non-physical values and erroneous data associated with spurious reflections from blowing snow.